J. Fluid Mech. (2005), *vol.* 529, *pp.* 1–32.
doi:10.1017/S0022112004002794 Printed in the United Kingdom

On the non-parallel instability of sediment-carrying channels of slowly varying width

By PHILIP HALL

Department of Mathematics, Imperial College, London SW7 2BZ, UK

(Received 16 September 2003 and in revised form 2 June 2004)

The flow of a river in a channel of slowly varying width is investigated using an asymptotic approach. The work was motivated by a recent experimental investigation of this problem. The river transports sediment as bedload and is susceptible to an instability which causes variations in the depth of the river. The asymptotic theory is, in the first instance, used to describe steady-state flows in channels of varying width and it is found to give excellent agreement with experimental observations on this flow. The theory shows conclusively that a river of slowly increasing width will form central bars. Secondly, the approach is used to investigate the instability of the flow. The major result obtained is that in a symmetric channel which diverges from a width where the flow is unstable to one where instability is possible, then the preferred mode of instability is likely to be a central bar rather than an alternating bar as is the case in straight channels.

1. Introduction

Our concern is with the development of bar instabilities in channel flows of slowly varying width. The work is motivated by the paper of Federici & Paola (2003, hereinafter referred to as FP). FP investigated the effect of channel divergence on bar formation. Various situations were investigated by the latter authors, but the one which we focus on here corresponds to the flow of a sediment-carrying fluid in a linearly divergent channel with rigid sidewalls. Related experiments were carried out by Bolla Pittaluga, Repetto & Tubino (2003) who investigated the stability of river bifurcations in gravel braided networks using a one-dimensional model. The latter paper is therefore relevant to the situation when the network is developed; here, our work is more relevant to the processes leading to a braided network. In a sequence of experiments FP found that divergence caused the generation of a central bar in the divergent part of the channel. The experiments with rigid sidewalls were designed such that the flow before the divergent reach was stable. Downstream of the divergent section of the channel, the flow was unstable, so between the upstream stable section and the unstable region downstream, the flow will be locally unstable to, in the first instance, alternating bar modes. In all situations, it was observed experimentally that the divergence of the channel caused central bars to develop in preference to the usual case where alternating bars form. In order to understand why this occurs, we will use a slowly varying approach to describe the basic steady-state configurations possible in a divergent channel and then go on to consider the instability of these flows. We now give a brief review of the most relevant previous investigations of bar instabilities.

The most significant original contributions to our understanding of migrating bar instabilities in channel flows are due to Leopold & Wolman (1957), Kinoshita (1961), Colombini, Seminara & Tubino (1987) and Seminara & Tubino (1990). The instability

arises because of the natural tendency of particles dragged along in a turbulent stream to form crests and troughs. The basic mechanism is responsible for a multitude of patterns formed on river beds, e.g. alternating bars and central bars, and in the nonlinear regime it is possibly responsible for braiding. The relationship between bar instabilities and meanders is still in doubt, but various authors (e.g. Blondeaux & Seminara 1985, hereinafter referred to as BS) have argued that there is a connection between the phenomena. Bars are thought to be the fundamental morphodynamic building blocks required to form meanders and braided beds and therefore have important consequences for river ecology and river training.

Hall (2004) investigated bar instabilities in unsteady flows and pointed out that these instabilities are convective in nature. Hall was therefore able to discuss the receptivity problem for bars. Here, the terminology comes from boundary-layer transition studies where receptivity has become known as the process by which temporal and spatial irregularities in a flow trigger disturbances. Moreover, the theory is able to predict the size of bar induced by particular obstacles. The convective nature of the bar instability problem was subsequently discussed in detail by Federici & Seminara (2003). The major property of a convectively unstable flow is that instability occurs because of the spatial evolution of a constant-frequency wave as it moves downstream. Flows which are absolutely unstable, on the other hand, behave differently with instability spreading out in all directions from a localized disturbance to the flow. Thus, in a sediment-carrying river, instability will arise when flow unsteadiness interacts with spatial irregularities to produce downstream propagating waves and the instability problem should therefore be discussed in terms of the spatial evolution of a constant-frequency input; that is the approach used here.

The experiments of FP were motivated by a desire to understand the mechanism which causes braiding in channels. Such systems have a variety of connected channels of different width. Ashmore (1982, 1991) investigated experimentally the possible mechanisms which cause braiding in an initially straight unconstrained cohesionless channel. Ashmore found that the initial stage is the generation of alternate bars which produce weak curvature variations of the channel. Subsequently, bank erosion causes local width variations of the channels and this ultimately leads to the generation of steady bars. Repetto, Tubino & Paola (2003) have looked at the instability of the flow in a wavy channel and their results suggest that width changes can cause the formation of steady central bars. The analysis was restricted to small-amplitude waviness and some discussion of that problem can be found in Hall (2004). Here, we are concerned with the experimental situation of FP where a channel diverges in width by a factor of 3 and the sidewalls are constrained.

The first part of our theory will be used to describe steady-state flows in divergent channels. We assume that the channel diverges slowly and use a multiple-scale approach to solve the flow equations asymptotically. The approach is similar to classical lubrication theory and at any location along the channel the flow is one which could occur in an infinitely long channel of the same width. However, it turns out that there is a global connection between the flows at different local stations and a nonlinear equation is derived to define this connection. The existence of this global connection makes it impossible for the instability problem to be discussed without taking it into account. The point we are making is that in a slowly-varying flow at any station, it is reasonable to expect that the flow should look like that which would occur in an infinitely long channel. However, there are an infinite number of such flows and the global constraint fixes which one is selected at any location so a stability theory applied to an arbitrary choice of solution would be meaningless.

The procedure adopted in this paper is as follows. In § 2, we summarize the equations of motion and the basic states describing rivers of slowly varying width. The structures we find are compared with experimental observations and used as the basis for our stability analysis in § 3. In § 4, we discuss our results and relate them to the experimental observations of FP.

2. Steady flows in channels of slowly varying width

Consider the flow in a channel of rectangular cross-section of width $2B_0^*$ and of typical depth D_0^*. If x^* and y^* denote variables along and normal to the midpoint of the channel, we define dimensionless variables x and y by

$$(x, y) = (x^*, y^*)/B_0^*, \tag{2.1}$$

and scale the corresponding velocity components on a typical speed U_0^* so that

$$(U, V) = (U^*, V^*)/U_0^*. \tag{2.2}$$

If H and D are the dimensionless water surface elevation and depth defined by

$$(H^*, D^*) = D_0^*\big(F_0^2 H, D\big), \tag{2.3}$$

where the Froude number F_0 is defined by

$$F_0^2 = \frac{U_0^{*2}}{gD_0^*}, \tag{2.4}$$

then the St Venant shallow-water equations take the form

$$U\frac{\partial U}{\partial x} + V\frac{\partial U}{\partial y} = -\frac{\partial H}{\partial x} - \frac{\beta\tau_x}{D}, \tag{2.5a}$$

$$U\frac{\partial V}{\partial x} + V\frac{\partial V}{\partial y} = -\frac{\partial H}{\partial y} - \frac{\beta\tau_y}{D}, \tag{2.5b}$$

$$\frac{\partial}{\partial x}(UD) + \frac{\partial}{\partial y}(VD) = 0. \tag{2.5c}$$

Here, $\beta = B_0^* D_0^{*-1}$ is the aspect ratio of the channel whilst τ_x, τ_y are the bottom shear stresses in the x and y directions and have been scaled on ρU_0^{*2}. The total dimensional stress on the bottom is therefore given by $\tau_0^* = \rho U_0^{*2}\sqrt{\tau_x^2 + \tau_y^2}$. In the above equations, turbulent effects have been averaged out and we have ignored dispersion effects associated with flow curvature. A referee has pointed out to the author that for flows with significant curvature, these effects might be important, but for sufficiently small values of ϵ that will not be the case. The excellent agreement we find between our predictions and the experiments of FP suggests that the assumption is valid for the values of ϵ used in this paper.

The sediment flow rates Q_x^* and Q_y^* are now made dimensionless using $\{((\rho_s - \rho)/\rho)gd_s^*\}^{1/2}$ as an appropriate scale. Here, ρ_s and ρ are the sediment and fluid densities and d_s^* is a typical sediment scale. Thus, we write

$$(Q_x^*, Q_y^*) = \left\{\frac{(\rho_s - \rho)}{\rho} g d_s^*\right\}^{1/2} (Q_x, Q_y). \tag{2.6}$$

The appropriate time variable t associated with the motion of the sediment is defined by

$$t^* = \frac{B_0^*}{U_0^*} t, \tag{2.7}$$

and then the equation of continuity for the sediment becomes

$$\frac{\partial}{\partial t}\left(F_0^2 H - D\right) + Q_0\left(\frac{\partial Q_x}{\partial x} + \frac{\partial Q_y}{\partial y}\right) = 0, \tag{2.8}$$

where

$$Q_0 = d_s^*\left\{\frac{(\rho_s - \rho)}{\rho} g d_s^*\right\}^{1/2} \Big/ ((1-p) D_0^* U_0^*), \tag{2.9}$$

with p denoting the sediment porosity. It should be noted here that the time-dependence of the system appears only explicitly in the sediment equation. Finally, the system of equations is closed by equations to determine the wall stresses and sediment flow rates. Following, for example, BS, we write

$$(\tau_x, \tau_y) = C(U, V)\sqrt{U^2 + V^2}, \tag{2.10}$$

$$C = \left[\frac{1}{6 + 2.5\ln(D/2.5d_s)}\right]^2, \quad d_s = \frac{d_s^*}{D_0^*}, \tag{2.11a, b}$$

$$(Q_x, Q_y) = (\cos\delta, \sin\delta)\Phi, \tag{2.12}$$

$$\sin\delta = \frac{V}{\sqrt{U^2 + V^2}} - \frac{r}{\beta\theta^{1/2}} \frac{\partial}{\partial y}\left(F_0^2 H - D\right). \tag{2.13}$$

The expression for C given by (2.11a) is due to Engelund & Hansen (1967) and is valid only for planar beds. Equation (2.13) is valid only if the sediment is transported mainly as bedload. (See BS for a full discussion of the assumptions and approximations which must be made in order to derive the above equations.) The bedload function Φ is defined by the Meyer–Peter–Muller formula:

$$\Phi = 8(\theta - 0.047)^{3/2}. \tag{2.14}$$

Here, θ is the Shield stress which is defined in terms of the total (dimensional) wall shear stress τ_0^* by

$$\theta = \frac{\tau_0^*}{(\rho_s - \rho) g d_s^*} = \Theta_0\sqrt{\tau_x^2 + \tau_y^2}, \tag{2.15}$$

$$\Theta_0 = \frac{\rho (U_0^*)^2}{(\rho_s - \rho) g d_s^*}. \tag{2.16}$$

The constant Θ_0 defined by (2.16) is, apart from a factor C, the Shield stress for the uniform flow $(U, V) = (1, 0)$.

We shall now determine the steady flow in a channel of slowly varying width. Suppose then that the channel is defined by

$$G(\epsilon x) \leqslant y \leqslant F(\epsilon x), \tag{2.17}$$

where ϵ is a small and positive parameter. For sufficiently small values of ϵ, the flow at any local station will not know that the channel is divergent and therefore we anticipate that the flow there will be predominantly in the x-direction. However, we cannot say how fast the flow will be at a local station without considering the global

problem. In order to do so, we use an expansion procedure which is essentially based on a lubrication theory approach.

We define $X = \epsilon x$ and seek a steady solution of the fluid and sediment equations in terms of X and y. Since the flow is slowly varying in the X-direction, we expect U to be only a function of X at leading order. The velocity components are therefore expanded as

$$U = \overline{U} = U_0(X) + \epsilon U_1(x, y) + \cdots, \tag{2.18a}$$

$$\frac{V}{\epsilon} = \overline{V} = V_0(X, y) + \epsilon V_1(X, y) + \cdots, \tag{2.18b}$$

where the $O(\epsilon)$ difference in velocity scales is implied by the equation of continuity written in terms of X and y.

The height H then expands as

$$H = \overline{H} = \frac{1}{\epsilon} H_0(X) + H_1(X) + \epsilon H_2(X, y) + \cdots, \tag{2.19}$$

and the depth D as

$$D = \overline{D} = D_0(X) + \epsilon D_1(X, y) + \cdots. \tag{2.20}$$

For small enough values of ϵ, we expect that at leading order the basic state will be locally identical to that in a uniform channel. Thus, we have anticipated that U_0, H_0 and D_0 depend only on X. Note that, locally, H_0 will be found to vary like X so in terms of the original streamwise coordinate $H \sim x$ which is the constant-width solution.

The leading-order approximations to the momentum, continuity and sediment equations yield

$$\frac{\partial H_0}{\partial X} = -\frac{\beta C_0(X) U_0^2(X)}{D_0(X)}, \tag{2.21a}$$

$$\frac{\partial}{\partial y}(H_0(X)) = 0, \tag{2.21b}$$

$$\frac{\partial}{\partial X}(U_0 D_0) + \frac{\partial}{\partial y}(V_0 D_0) = 0, \tag{2.21c}$$

$$\frac{\partial \Phi_0}{\partial X} + \frac{\partial}{\partial y}\left\{ \Phi_0 \left(\frac{V_0}{U_0} - J_0 \right) \left[F_0^2 H_2 - D_1 \right] y \right\} = 0. \tag{2.21d}$$

Here, $C_0(X) = C_0(D = D_0)$ and $J_0 = r/(\beta \theta_0^{1/2} C_0^{1/2} U_0)$. The above equations must be solved subject to:

$$V_0 - F'(X) U_0 = 0, \quad y = F, \tag{2.22a}$$

$$V_0 - G'(X) U_0 = 0, \quad y = G, \tag{2.22b}$$

so that the normal velocity vanishes at the boundaries. The condition that there is no flow of sediment normal to the boundary gives

$$\frac{\partial}{\partial y}\left[F_0^2 H_2 - D_1 \right] = 0, \quad y = F,\ G. \tag{2.22c, d}$$

If we integrate (2.21*d*) from $y = G$ to $y = F$ and use (2.22), we obtain

$$\frac{\partial}{\partial X}(\Phi_0 [F - G]) = 0 \tag{2.23}$$

so that

$$\Phi_0(F-G) = 2\Phi_0, \tag{2.24}$$

where Φ_0 is the bedload function for a uniform flow $U_0 = D_0 = 1$.

Similarly, if we integrate the equation of continuity from $y = G$ to $y = F$ and use (2.22) we deduce that

$$U_0 D_0 (F-G) = \text{constant}, \tag{2.25}$$

and we can take the constant to be 2 so that (2.25) reduces to the uniform flow solution $U_0 = D_0 = 1$ when $F = 1, G = -1$. Since F and G are given functions of X it follows that (2.25) relates U_0 and D_0. However, we still do not have enough information to find these quantities independently.

We further note that the sediment flow equation integrated from G to y yields

$$\left(\frac{y-G}{F-G}\right)(\Phi_0[F-G])_X = \Phi_0 J_0 \frac{\partial}{\partial y}\left[F_0^2 H_2 - D_1\right], \tag{2.26}$$

so that, using (2.24), $(\partial/\partial y)[F_0^2 H_2 - D_1]$ is found to be identically zero in $G < y < F$. Hence,

$$F_0^2 \frac{\partial H_2}{\partial y} = \frac{\partial D_1}{\partial y}. \tag{2.27}$$

Equations (2.24) and (2.25) then determine $U_0(X)$ or $D_0(X)$ implicitly for a given channel geometry. We see that the solution depends only on the width of the channel $F-G$ rather than on F and G independently. Note, however, that the restriction that $\epsilon \ll 1$ means that there is no possibility of flow separation since U_0 must remain positive above. This solution procedure can be extended to arbitrary order, but the details become somewhat tedious. For brevity, here we simply state the results which emerge from the next order approximation to the momentum, continuity and sediment flow equation when solved subject to the appropriate boundary conditions. First, we find that H_1 is a function of X only and in fact

$$\frac{\mathrm{d}H_1}{\mathrm{d}X} = U_0 U_{0X}. \tag{2.28}$$

The function D_1 is given by

$$D_1 = \frac{F_0^2 \beta C_0 U_0}{D_0}\left[\int_G^y V_0 \,\mathrm{d}y - \frac{\int_G^F \mathrm{d}\tilde{y} \int_G^{\tilde{y}} V_0}{F-G}\,\mathrm{d}y\right], \tag{2.29a}$$

which incidently means that

$$\int_G^F D_1 \,\mathrm{d}y = 0 = \int_G^F U_1 \,\mathrm{d}y, \tag{2.29b}$$

so that there is no $O(\epsilon)$ change to the mean value of D. The streamwise and normal velocity components then follow from

$$U_1 = -\left\{\frac{C_0' U_0 - U_0 C_0 D_0^{-1}}{2C_0}\right\} D_1 = A(X) D_1, \tag{2.30a}$$

$$D_0 V_1 = -\int_G^y \{U_1 D_0 + U_0 D_1\}_X - [V_0 D_1]_G^y. \tag{2.30b}$$

Finally, the transverse variation of the order ϵ^2 sediment depth is found to be given by

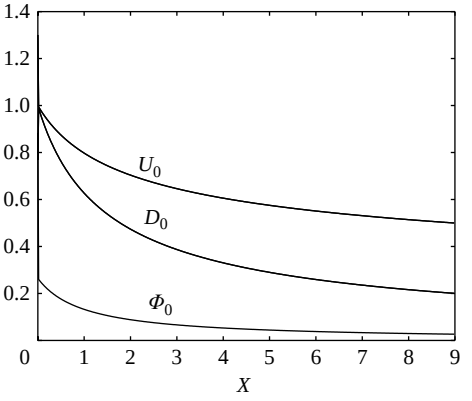

FIGURE 1. The dependence of U_0, D_0, Φ_0 on X for $d_s = 0.05$, $C_0\Theta_0 = 0.15$.

$$\int_G^y \frac{\partial}{\partial X}\{\Phi_0'\Theta_0[C_0'U_0^2D_1 + 2C_0U_0U_1]\}\,\mathrm{d}y - \left[\frac{V_0}{U_0}\Phi_0'\Theta_0(C_0'U_0^2D_1 + 2C_0U_0U_1)\right]_G^y + \left\{\Phi_0\left[\frac{V_1}{U_0} - \frac{V_0U_1}{U_0^2}\right]\right\}_G^y = J_0\frac{\partial}{\partial y}\{F_0^2H_3 - D_2\}. \quad (2.31)$$

The vanishing of the integrals of the depth and streamwise velocity corrections at order ϵ means that, correct to order ϵ, their effects on the mean values of these flow quantities also vanish so that when we compare with experiments, then correct to $O(\epsilon)$, we can ignore these corrections.

Equation (2.31) fixes the shape of the bedform induced by the change in channel width. Note that H_0 and D_0 are functions of X only whilst $(\partial/\partial y)\{F_0^2H_2 - D_1\} = 0$, so that the first spanwise variation of the sediment depth occurs at $O(\epsilon^2)$ and is therefore fixed by $(\partial/\partial y)\{F_0^2H_3 - D_2\}$. Before we present some solutions of these equations, we note that we restrict our attention to situations with $\theta > 0.047$ so that there is always transport of sediment taking place. If this is not the case, $F_0^2H - D$ is constant and the X momentum equation is integrated to find H in terms of D and U. The resulting equation is then solved subject to (2.25).

We first consider the flow in a divergent channel with linearly increasing width defined by

$$\left.\begin{aligned} y &= \pm 1, \quad X < 0, \\ y &= \pm(1 + X), \quad X > 0. \end{aligned}\right\} \quad (2.32)$$

This channel is of particular interest because FP have performed experiments in such a channel. In the experiments, which will be discussed in more detail later, the walls of the channel were inclined at angles α up to about 15° to the mid-plane of the channel. Thus, ϵ corresponds to $\tan\alpha$ and is therefore numerically small in the experiments so we might expect that our theory is applicable to them.

Figure 1 shows $U_0(X)$, $D_0(X)$ and $\Phi_0(X)$ calculated for the case $\Theta_0C_0 = 0.15$, $d_s = 0.05$ which is typical of the values used in the experiments. We observe that all these quantities decrease as X increases. Figure 2 shows the variation of $\beta_\Delta = (F(X) - G(X))/2D_0(X)$, $\Omega_\Delta = ((F(X) - G(X)))/2U_0(X)$, with X whilst figure 3 shows β_Δ as a function of Ω_Δ. We shall see later that β_Δ, a local aspect ratio per unit initial β, and Ω_Δ, a local frequency parameter, for a time periodic initial disturbance of unit frequency at $X = 0$ play crucial roles in the stability problem. In fact, the dependence

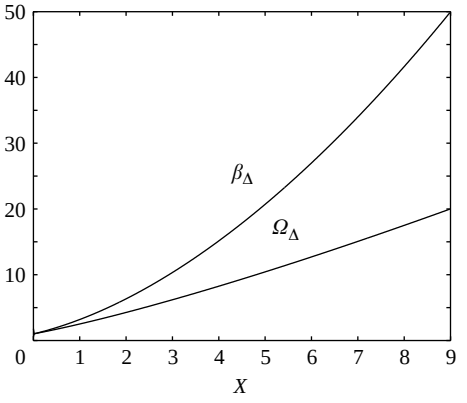

FIGURE 2. The dependence of β_Δ, Ω_Δ on X for $d_s = 0.05$, $C_0\Theta_0 = 0.15$.

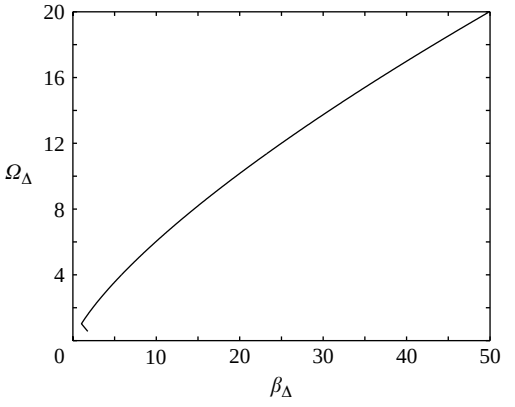

FIGURE 3. The dependence of β_Δ on Ω_Δ for $d_s = 0.05$, $C_0\Theta_0 = 0.15$.

of β_Δ on Ω_Δ determines the path in the β-frequency plane of a constant-frequency wave as it moves downstream. This path is the crucial input to the stability problem for a wave propagating in a channel of slowly varying width.

FP carried out measurements in channels defined by (2.32) for $X \leqslant 2$. The width of the channel therefore increases by a factor of 3 in the divergent section. The values of the parameters used in those experiments are given in table 3 of that paper. Note that only the first eight experiments of FP are relevant to the present situation, since they alone correspond to rigid banks. In order to compare our predictions, we note that in those experiments, the channel width increased by a factor of 3 before becoming straight again. FP found the ratios of the local β terms at the exit and entrance to be 30/6, 27/4.5, 19/3, 60/10, 30/5, 43/7, 21/3 and 13/2. This ratio corresponds to $\beta_\Delta(2)$ in our notation. This ratio is approximately 6.4, which agrees well with the experimental results. Note here that if we are working correct up to $O(\epsilon)$, we can ignore the $O(\epsilon)$ corrections to U_1 and D_1 since they were shown earlier to have zero mean. Note, however, that the experimental runs used sand with a typical scale of 0.01 m and different upstream fluid depths, so strictly speaking it is not valid to compare the experiments with figure 2 which we calculated with $d_s = 0.05$. However, the dependence of the results on this quantity is weak and figure 4 shows

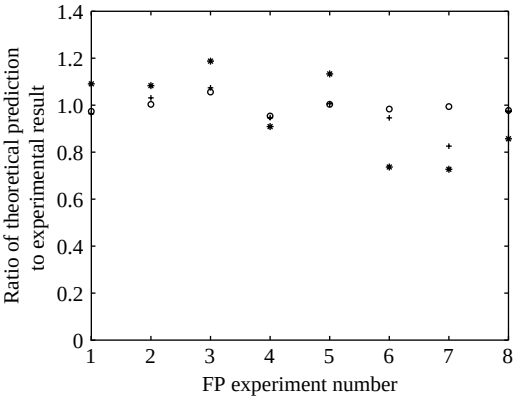

FIGURE 4. Comparison of theory with FP experimental results. ○, β; +, Froude number; ∗, wall stress.

the correct comparison between theory and experiment. Case 1 of FP corresponds to $\epsilon = \tan(\alpha)$ with $\alpha = 10^\circ$ and the other results correspond to $\alpha = 15^\circ$ which suggests that our slowly varying approach should be relevant and indeed, figure 4 shows a remarkably good agreement between theory and experiment. For most of the comparisons, we see that the error is less than 10% and only in a few cases it is about 20%. It is crucial to note here that our theory is based on the assumption that locally the flow is essentially in the X-direction. However, the strength of the flow and the local fluid depth and free-surface elevation also come out of a global calculation. This is crucial because without this knowledge a quasi-parallel stability theory cannot be carried out. The experiments of FP showed that in the divergent part of a channel flow with symmetric sidewalls of constant slope, a central bar was formed. Our calculation above showed that at leading order, the basic state is identical to that in an infinitely long channel with width equal to the local width of the channel, so there is no possibility of a bar structure. Now let us consider the flow pattern and sediment depth associated with the higher-order effect calculated above. The local sediment depth is given by

$$S_d = B_0^* \left(F_0^2 \left[\frac{1}{\epsilon} H_0(X) + H_1(X) + \epsilon H_2(X, y) + \cdots \right] - D_0(X) - \epsilon^2 D_1(X, y) - \cdots \right).$$

Hence, the spanwise slope of the sediment is given by S_{dl} where $S_{dl} = (F_0^2[\epsilon^2 H_3(X, y) + \cdots] - \epsilon^2 D_2(X, y))_y$. Note here that though H_2 and D_1 depend on y, the combination $F_0^2 H_2(X, y) - D_1(X, y)$ is independent of y, so that spanwise variations of sediment occur first at $O(\epsilon^2)$. We also stress that if we wish to plot the sediment depth correct to $O(\epsilon^2)$ rather than its spanwise derivative, then the expansion procedure given above has to be continued to two further orders of magnitude in ϵ; in principle, that causes no difficulty, but the calculation becomes inordinately tedious and, as pointed out by other authors, the validity of the model we are using for sediment transport does not warrant a calculation to such order. Moreover, the spanwise slope of sediment depth fixes the shape of any forced bar, so we are able to make a comparison with FP without continuing the expansion procedure to higher order. Figure 5 plots contours of constant spanwise slope of sediment in the divergent reaches of the experiments 1–8 of FP. In all cases, the slope is negative in the top half of the channel and positive elsewhere. The slope vanishes along the centreline and

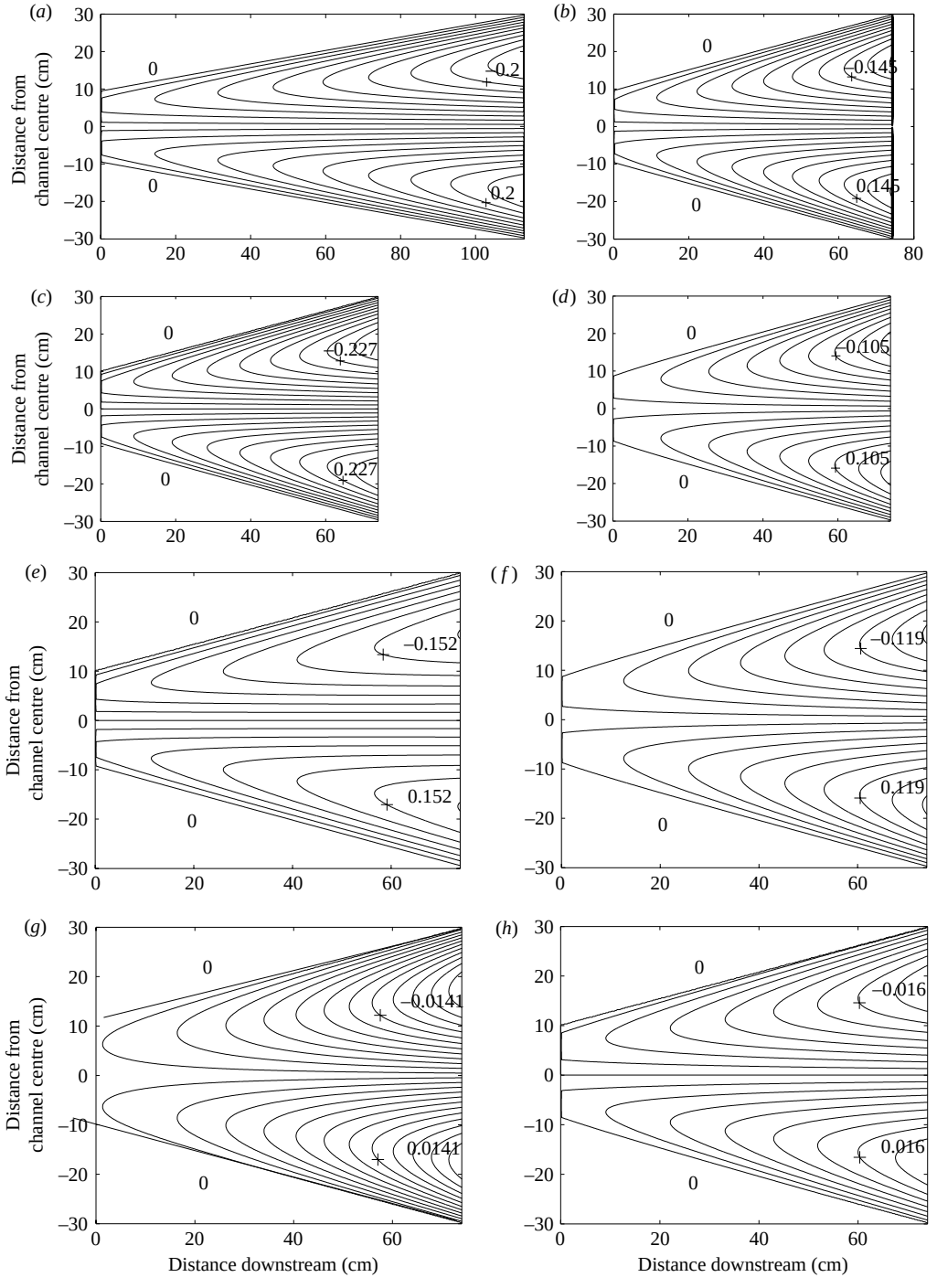

FIGURE 5. (*a–h*) Contours of constant spanwise slope of sediment in FP experiments 1–8.

channel walls. When y increases from zero along the centreline, the slope decreases until it reaches a negative minimum and then increases until it reaches zero. Thus, our results accurately predict the central bar structure found in the experiments.

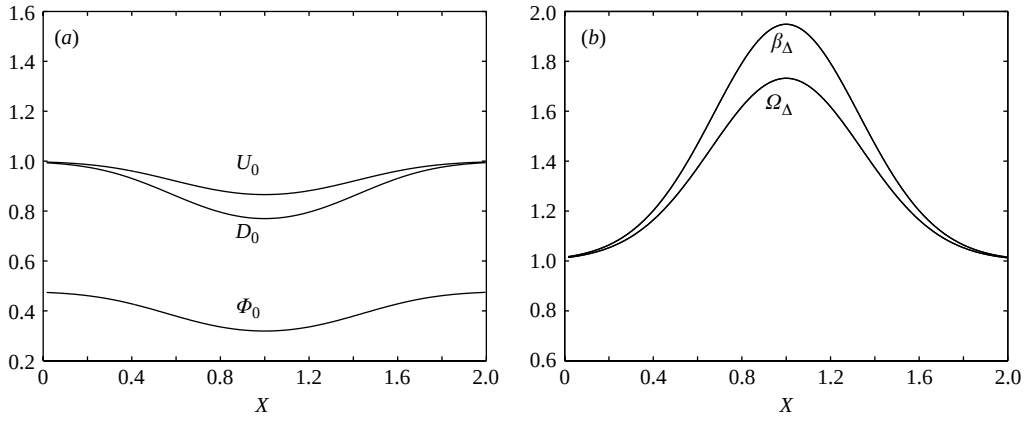

FIGURE 6. The dependence of (*a*) U_0, D_0, Φ_0 and (*b*) β_Δ, Ω_Δ on X for $d_s = 0.05$, $C_0\Theta_0 = 0.15$ for the dilated channel.

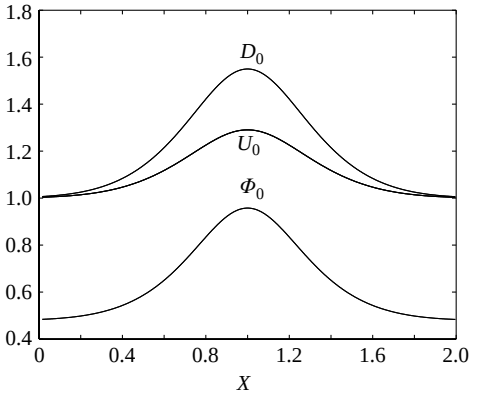

FIGURE 7. The dependence of U_0, D_0, Φ_0 on X for $d_s = 0.05$, $C_0\Theta_0 = 0.15$ for the constricted channel.

Now consider the channel with walls defined by

$$y = \pm(1 + A\exp(-4(X-1)^2)), \quad -\infty < X,$$

where A is a constant and positive/negative values of A represent dilated/constricted channels.

In the first instance, let us consider the dilated case and take $A = 0.5$ so that the maximum width is 3/2 times the minimum one. Figure 6(*a*) shows the dependence of U_0, D_0 and Φ_0 on X. The channel is symmetric about $X = 1$ and this symmetry is maintained by the flow properties plotted. Figure 6(*b*) shows the dependences of β_Δ and Ω_Δ on X. We see that the local value of the aspect ratio increases by about a factor of 2 as the channel increases in width by a factor 1.5. The corresponding increase in Ω_Δ is somewhat less in magnitude. Figures 7 and 8 show the corresponding results for the constricted channel. Here, the local aspect ratio falls by a factor of 3 when the channel width decreases by a factor of 2. In both cases, we observe that $\beta_\Delta/\Omega_\Delta$ is nearly constant, as was found to be the case for the divergent channel.

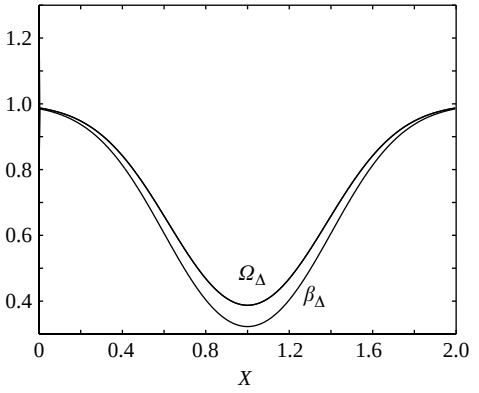

FIGURE 8. The dependence of β_Δ, Ω_Δ on X for $d_s = 0.05$, $C_0\Theta_0 = 0.15$ for the constricted channel.

3. The non-parallel instability of channel flows

We have seen that flow divergence leads to a steady basic state which has a central bar in the divergent part of the channel. In the divergent part of the channel, the local width ratio increases beyond the value at which bar instabilities might be expected to form and we now address the instability problem. Note, however, that in channels where the background level of disturbance is large the weak central bar associated with flow divergence may not be formed because much larger amplitude structures associated with an instability can grow and swamp the forced steady central bar.

Let us consider the instability of the basic state $(U, V, H, D) = (\overline{U}, \epsilon\overline{V}, \overline{H}/\epsilon, \overline{D})$ discussed in the previous section. Suppose that the corresponding values of $\Phi, \theta, \tau_x, \tau_y, \tau_s$ are denoted by $\overline{\Phi}, \overline{\theta}, \overline{\tau}_x, \overline{\tau}_y$ and $\overline{\tau}_s$, respectively. The appropriate expansions of these functions are

$$\left.\begin{aligned} &\Phi = \Phi_0(X) + O(\epsilon), \quad \overline{\theta} = \theta_0(X) + O(\epsilon), \quad \overline{\tau}_x = \overline{\tau}_{x0}(X) + O(\epsilon), \\ &\overline{\tau}_y = \overline{\tau}_{y0}(X) + O(\epsilon), \quad \overline{\tau}_s = \overline{\tau}_{s0}(X) + O(\epsilon). \end{aligned}\right\} \tag{3.1}$$

We assume at this stage that the disturbances to be imposed on the flow are small compared to any power of ϵ. (In other words the background disturbance field is arbitrarily small.) The instability operates on a spatial length scale comparable with the channel width, so we use a WKB formulation which allows for a wave of slowly varying wavenumber of wavelength $O(B_0^*)$ to propagate in the flow direction. We first perturb the basic state of § 2 by writing

$$\left.\begin{aligned} &U = \overline{U} + \widetilde{U}(X, y; \epsilon), \quad \frac{V}{\epsilon} = \overline{V} + \frac{\widetilde{V}}{\epsilon}(X, y; \epsilon), \quad \theta = \overline{\theta} + \widetilde{\theta}(X, y; \epsilon), \\ &\tau_x = \overline{\tau}_x + \widetilde{\tau}_x(X, y; \epsilon), \quad \frac{\tau_y}{\epsilon} = \overline{\tau}_y + \frac{\widetilde{\tau}_y}{\epsilon}(X, y; \epsilon), \quad \Phi = \overline{\Phi} + \widetilde{\Phi}(X, y; \epsilon), \\ &H = \overline{H} + \widetilde{H}, \quad D = \overline{D} + \epsilon\widetilde{D}. \end{aligned}\right\}. \tag{3.2}$$

Here, we assume $\widetilde{U}$, $\widetilde{V}$ etc. are small so that the linearized form of (2.5) becomes

$$\epsilon\overline{U}\frac{\partial\widetilde{U}}{\partial X} + \epsilon\widetilde{U}\frac{\partial\overline{U}}{\partial X} + \epsilon\overline{V}\frac{\partial\widetilde{U}}{\partial y} + \widetilde{V}\frac{\partial\overline{U}}{\partial y} = -\epsilon\frac{\partial\widetilde{H}}{\partial X} - \beta\left(\frac{\widetilde{\tau}_x}{\overline{D}} - \frac{\overline{\tau}_x\widetilde{D}}{\overline{D}^2}\right), \tag{3.3a}$$

$$\epsilon^2\widetilde{U}\frac{\partial\overline{V}}{\partial X}+\epsilon\overline{U}\frac{\partial\widetilde{V}}{\partial X}+\epsilon\overline{V}\frac{\partial\widetilde{V}}{\partial y}+\epsilon\widetilde{V}\frac{\partial\overline{V}}{\partial y}=-\frac{\partial\widetilde{H}}{\partial y}-\beta\left(\frac{\widetilde{\tau}_y}{\overline{D}}-\frac{\overline{\tau}_y\widetilde{D}}{\overline{D}^2}\right), \tag{3.3b}$$

$$\epsilon\left[\overline{U}\frac{\partial\widetilde{D}}{\partial X}+\widetilde{U}\frac{\partial\overline{D}}{\partial X}+\widetilde{D}\frac{\partial\overline{U}}{\partial X}+\overline{D}\frac{\partial\widetilde{U}}{\partial X}\right]+\widetilde{V}\frac{\partial\overline{D}}{\partial y}+\overline{D}\frac{\partial\widetilde{V}}{\partial y}+\epsilon\overline{V}\frac{\partial\widetilde{D}}{\partial y}+\epsilon\widetilde{D}\frac{\partial\overline{V}}{\partial y}=0. \tag{3.3c}$$

Finally, the perturbed form of the sediment continuity equation becomes

$$\frac{\partial}{\partial t}\left(F_0^2\widetilde{H}-\widetilde{D}\right)+Q_0\left(\epsilon\frac{\partial\widetilde{Q}_x}{\partial X}+\frac{\partial\widetilde{Q}_y}{\partial y}\right)=0. \tag{3.4}$$

Here, $\widetilde{Q}_x$ and $\widetilde{Q}_y$ are the perturbations in Q_x and Q_y, respectively.

It is instructive at this stage to review the existing linear stability theory for alternating bars. In fact, we will point out some key features of the latter problem which have apparently been overlooked. It turns out that these features play a crucial role in the non-parallel problem. If the walls of the channel are straight, (2.5) supports a steady unidirectional flow solution $U=1$, $V=0$ with $D=1$. If this equilibrium state is perturbed to a travelling-wave disturbance of wavenumber α and frequency Ω we find that, following BS, the eigen relation may be written in the form

$$-\frac{\mathrm{i}\Omega}{Q_0}=-\Phi_0\frac{r}{\beta}M^2+\frac{(A_1\alpha^3+\mathrm{i}A_2\alpha^2+A_3\alpha+\mathrm{i}A_4)\alpha}{B_0+\mathrm{i}B_1\alpha+B_2\alpha^2+\mathrm{i}B_3\alpha^3}. \tag{3.5}$$

The constants A_1, A_2, etc. appearing above may be written in the form

$$A_1=f_1-f_2,\ A_2=-A_1\chi_0,\ A_3=(f_2-\Phi_0)M^2, \tag{3.6a–c}$$

$$A_4=-A_1M^2\chi_0s_1-M^2(\Phi_0-f_1)(s_2-s_1-1)\chi_0, \tag{3.6d}$$

$$B_3=F_0^2-1,\ B_2=-\left[\chi_0+F_0^2\chi_0(s_2-s_1-2)\right],\ B_1=-M^2+F_0^2\chi_0^2(s_2-s_1-1), \tag{3.6e–g}$$

$$B_0=-M^2\chi_0s_1,\ M=\frac{m\pi}{2},\ \chi_0=\beta C, \tag{3.6h–j}$$

where f_1, f_2 etc. are as defined in BS.

Previous investigators have used (3.5) to determine the complex frequency associated with a disturbance of (real) wavelength $2\pi/\alpha$. The neutral case is fixed by solving (3.5) with both α and Ω real for given values $m=1, 2, 3, 4, \ldots$ of the mode number. Note that odd/even values of m correspond to disturbance fields with the spanwise velocity even/odd about the centre, respectively. In particular, $m=1, 2$ correspond to alternating and central bars, respectively. The most dangerous mode corresponds to the case $m=1$ and, for all physically relevant values of the parameters of the problem, the neutral curves have been found to be of shapes shown in figure 9 with a critical wavenumber $\simeq 0.5$ and a critical aspect ratio $\simeq 10$. The neutral curves shown in figure 9 have been calculated with $F_0=\sqrt{1/2}$, $\Phi_0=0.3$, $r=0.3$, $\Theta_0=0.3$, and $d_s=0.01$. The curves are changed little if F_0, Φ_0 and θ are varied.

The frequency Ω is found to be positive (corresponding to downstream propagating waves) everywhere except at very small wavenumbers (typically $\alpha<0.1$). BS have argued that the stationary wave corresponding to the zero frequency mode might play a crucial role in the formation of bends.

In fact, it is now known from Hall (2004) that (3.5) is the eigenrelation corresponding to a convective instability so should therefore be solved for a complex value of α with the frequency real. Disturbances then grow or decay as they propagate

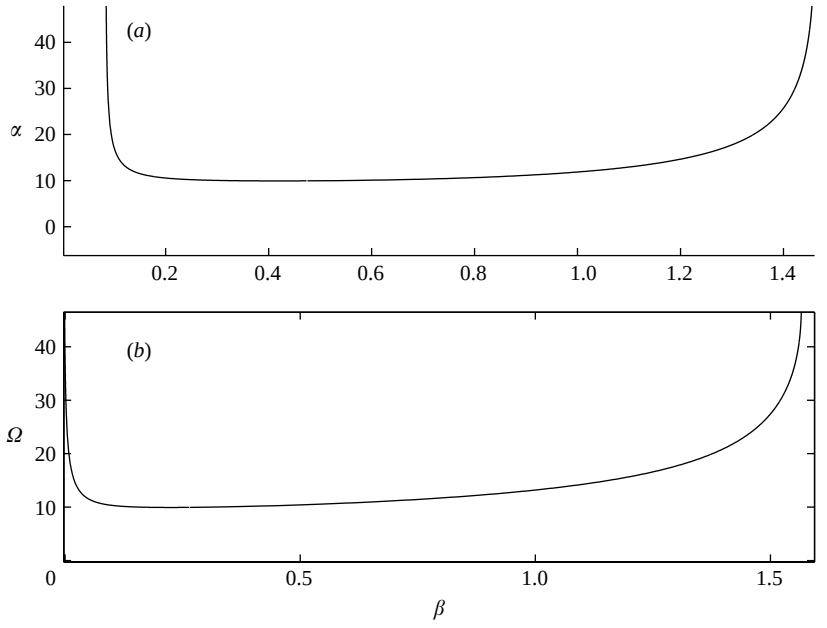

FIGURE 9. The neutral curves in (a) the (α, β)-plane and (b) the (Ω, β)-plane $\Theta_0 = 0.3$, $d_s = 0.01$, $\Phi_0 = 0.3$.

downstream of the position where they are stimulated in exactly the same way that Tollmien–Schlichting waves develop downstream of a vibrating ribbon in a growing boundary layer (see Gaster 1974). Of course, the neutral configuration is independent of whether we use spatial or temporal instability theory since α and Ω are then both real.

It appears that the nature of (3.5) at large values of the aspect ratio β has not been discussed. It might appear at first sight that the large-aspect-ratio limit is of no physical interest because the flow will be highly nonlinear by that stage. However, the structure found in this limit is crucial to our understanding of how a constant-frequency wave changes as it moves downstream. In fact, it is straightforward to find the large β forms of the neutral curve directly from (3.5). First, we note that on the left-hand branch of the neutral curve, the wavenumber and frequency both approach zero like β^{-1} and the appropriate asymptotic structure is

$$\alpha = \frac{\widehat{\alpha}}{\beta} + \cdots, \quad \Omega = \frac{\widehat{\Omega}}{\beta} + \cdots,$$

with

$$\widehat{\alpha}^2 = \Phi_0 \frac{rM^2 \widehat{B}_0}{\widehat{B}_{11} \widehat{A}_4}, \quad \widehat{\Omega} = -\frac{\widehat{A}_4 \widehat{\alpha} Q_0}{B_0},$$

where

$$B_0 = \beta \widehat{B}_0, \quad B_1 = \beta^2 \widehat{B}_{11} + \widehat{B}_{12}, \quad A_4 = \beta \widehat{A}_4 + A_{41}.$$

The right-hand branch of the neutral curve has the asymptotic behaviour

$$\Omega = \frac{\widehat{\Omega}}{\beta^2} + \cdots, \quad \alpha = \widehat{\alpha} + \cdots,$$

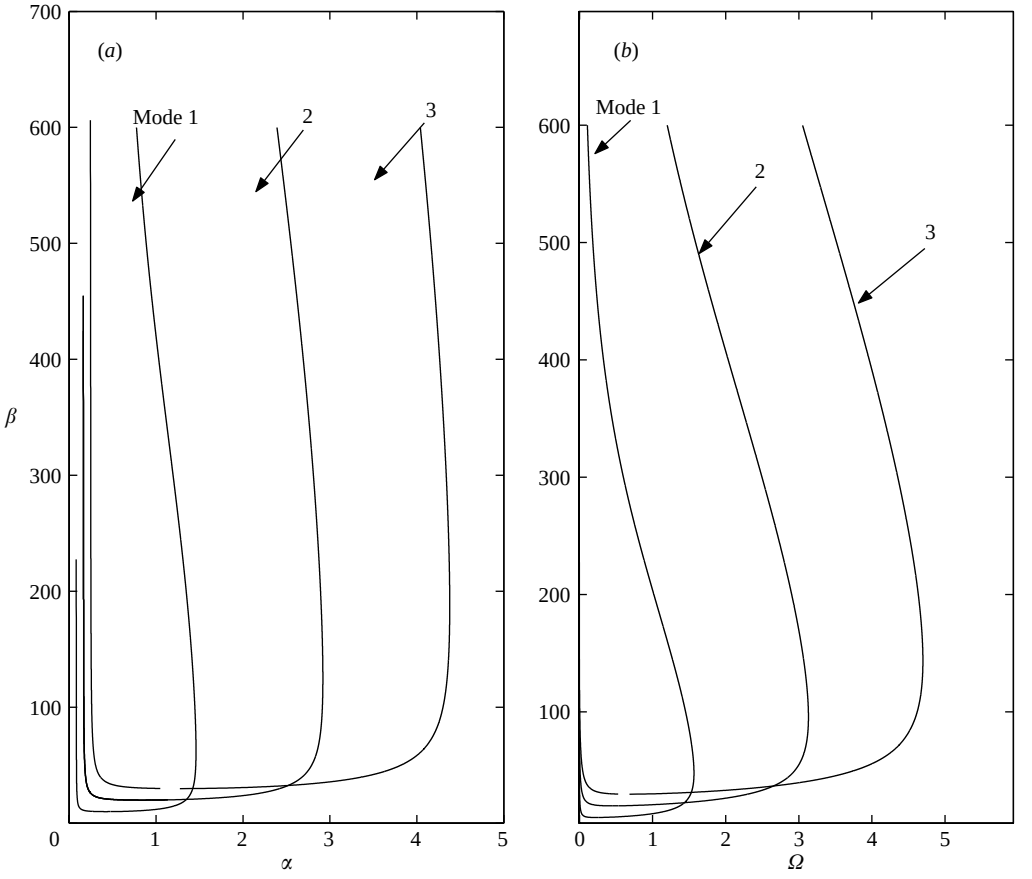

FIGURE 10. The first three neutral modes for the case of figure 9.

with

$$\widehat{\alpha}^2 = -\frac{\widehat{B}_{11}\Phi_0 r M^2 - \widehat{A}_4}{\widehat{A}_2}$$

$$-\frac{\widehat{\Omega}}{Q_0} = \frac{\widehat{A}_2\widehat{\alpha}^2 + \widehat{A}_4}{\widehat{B}_{11}}\left[-\left(\frac{\widehat{A}_1\widehat{\alpha}^3 + \widehat{A}_3\widehat{\alpha}}{\widehat{A}_2\alpha^2 + \widehat{A}_4}\right) + \left(\frac{\widehat{B}_0 + \widehat{B}_2\widehat{\alpha}^2}{\widehat{B}_{11}}\right)\right],$$

where $A_2 = \beta\widehat{A}_2$, $B_2 = \beta\widehat{B}_2$.

It is easy to show that for physically realistic values of the flow parameters the wavenumber $\widehat{\alpha}$ is to the left of the point on the neutral curve where $\mathrm{d}\alpha/\mathrm{d}\beta = 0$. In addition, it should be noted that the frequency Ω tends to zero on the right-hand branch of the neutral curves. Figure 10 shows the first 3 neutral modes of the eigenvalue problem. We see that the minimum values of β on each curve increases with the mode number and that as the frequency increases each mode becomes stable at all values of β.

In fact, figure 10 contains enough information for us to draw some highly significant conclusions about the non-parallel stability problem. Since the alternating bar instability is a convective one, it is appropriate to consider the spatial evolution

of a wave of constant frequency Ω. At the local position X, the local frequency based on the channel width there is defined by

$$\Omega_L = \Omega(F(X) - G(X))/\overline{U}(X) = \Omega\Omega_\Delta$$

and β_L the local value of the aspect ratio is defined by

$$\beta_L = \beta\frac{(f(X) - G(X))}{2\overline{D}(X)} = \beta\beta_\Delta. \tag{3.7}$$

Since the eigenrelation is only weakly dependent on Θ_0, Φ_0, F_0 (note that the eigenrelation will depend on the local values of these quantities as a wave moves downstream), it follows that the downstream path of a constant-frequency wave is approximately traced out by Ω_Δ as a function of β_Δ in the (Ω, β) plane. We saw earlier that in a linearly diverging channel this path moves away from the origin with β_Δ increasing slightly faster than Ω_Δ. This is also the case for the expanding parts of the constricted and dilated channel cases discussed earlier. Calculations with other geometries show that this result is typical with β_Δ increasing slightly faster than Ω_Δ as X increases through an expanding region. Thus, any wave will begin as a stable wave near the origin if β is sufficiently small and then pass into the unstable region of mode $m (m = 1, 2, 3 \ldots)$ before stabilizing to this mode. The flow is then unstable to the $m = 1$ mode before it stabilizes, and so on. Of course, the most important case is $m = 1$ and we see that in a channel which diverges, the first mode remains unstable for only a finite distance before the $M = 2$ mode takes over. Of course, this discussion ignores nonlinear effects, but nonlinearity will only alter the position where the $m = 2$ mode takes over.

The above approximate description of the non-parallel stability problem will now be set within the context of a formal expansion procedure capable of being extended, in principle, to any order in the small parameter ϵ characterizing the rate of change of channel width.

In order to take non-parallel effects into account in a self-consistent manner, we seek a WKB solution for $\widetilde{U}$ of the form

$$\widetilde{U} = \left\{\exp\left(-\mathrm{i}\Omega t + \frac{\mathrm{i}}{\epsilon}\int^X \alpha(s)\,\mathrm{d}s\right)\{U_0(X, y) + \epsilon U_1(X, y) + \ldots\} + \text{complex conjugate}, \right. \tag{3.8}$$

together with similar expansions for $\widetilde{V}$, $\widetilde{D}$, etc.

The frequency Ω in (3.8) is constant and the complex wavenumber α will vary with X as the wave moves downstream. Note also that F_0, β, θ_0 and Φ_0 are held fixed in the stability analysis, but that the eigenvalue problem will reflect the 'local' nature of these variables through the variation of the basic state variables with X. If the flow is parallel, (3.8) will reduce to the usual situation with α constant. Otherwise, α will vary and local growth rates and wavenumbers must be defined in terms of the disturbance field.

3.1. *Boundary conditions*

If the normal velocity is to vanish at the banks then, correct up to $O(\epsilon)$, we require that

$$\widetilde{V} - \epsilon F'(X)\widetilde{U} = 0, \quad y = F, \tag{3.9a}$$

$$\widetilde{V} - \epsilon G'(X)\widetilde{U} = 0, \quad y = G, \tag{3.9b}$$

whilst the condition that there should be no flow of sediment normal to the banks gives, correct to $O(\epsilon)$,

$$\frac{\partial}{\partial y}\left(F_0^2\widetilde{H}-\widetilde{D}\right)=0, \quad y=F, G. \tag{3.10}$$

The expansions for $\widetilde{U}, \widetilde{V}, \widetilde{D}$ and $\widetilde{H}$ are substituted into (3.3) and (3.4) and like powers of ϵ equated. At zeroth order, we find that

$$\mathrm{i}\alpha\overline{U}_0U_0+\mathrm{i}\alpha H_0+\frac{\beta}{\overline{D}_0}\overline{C}_0\{s_1U_0+s_2D_0\}-\frac{\beta\overline{C}_0\overline{U}_0^2}{\overline{D}_0^2}D_0=0, \tag{3.11a}$$

$$\mathrm{i}\alpha\overline{U}_0V_0+\frac{\partial H_0}{\partial y}+\frac{\beta}{\overline{D}_0}V_0\overline{C}_0\overline{U}_0=0, \tag{3.11b}$$

$$\mathrm{i}\alpha(\overline{U}_0D_0+\overline{D}_0U_0)+\overline{D}_0V_{0y}=0, \tag{3.11c}$$

$$-\frac{\mathrm{i}\Omega}{Q_0}\left(F_0^2H_0-D_0\right)+\mathrm{i}\alpha\overline{\Phi}_0(f_1U_0+f_2D_0)+\overline{\Phi}_0\left(\frac{V_{0y}}{\overline{U}_0}-R\frac{\partial^2}{\partial y^2}\left(F_0^2H_0-D_0\right)\right)=0, \tag{3.11d}$$

Here, the constants s_1, s_2, f_1 and f_2 are defined by

$$s_1=2\overline{U}_0, \quad s_2=\overline{U}_0^2\frac{\frac{\partial\overline{C}_0}{\partial\overline{D}_0}}{\overline{C}_0}, \quad f_1=\frac{2\Theta_0}{\overline{\Phi}_0}\overline{U}_0\overline{C}_0\overline{\Phi}_0', \quad f_2=\frac{\overline{U}_0^2\Theta_0}{\overline{\Phi}_0}\frac{\partial\overline{C}_0}{\partial\overline{D}_0}\overline{\Phi}_0'. \tag{3.12(a–d)}$$

The boundary conditions allow (3.11) to have a solution of the form

$$(U_0, V_0, H_0, D_0)=\widehat{h}_0(X)(\widehat{u}_0\mathscr{S}, \widehat{v}_0\mathscr{C}, \mathscr{S}, \widehat{d}_0\mathscr{S}), \tag{3.13}$$

where $\widehat{u}_0$, $\widehat{v}_0$, etc. are functions only of X and

$$\mathscr{S}=\sin\frac{m\pi\widehat{y}}{2}, \quad \mathscr{C}=\cos\frac{m\pi\widehat{y}}{2}, \quad m=1, 3, \ldots, \quad \widehat{y}=\frac{y-(F+G)/2}{(F-G)/2}.$$

We have anticipated above that the most dangerous mode has V_0 an even function of $\widehat{y}$ which measures distance from the midpoint of the walls. For convenience we now define

$$M=\frac{m\pi}{(F-G)}.$$

The equations (3.11) and (3.13) can then be used to write down the leading-order eigenrelation in the form

$$-\mathrm{i}\Omega=-\frac{\overline{\Phi}_0Q_0}{F_0^2-\widehat{d}_0}\left\{-\frac{\widehat{v}_0M}{\overline{U}_0}+RM^2\left(F_0^2-\widehat{d}_0\right)+\mathrm{i}\alpha(f_1\widehat{u}_0+f_2\widehat{d}_0)\right\}, \tag{3.14}$$

with

$$\widehat{v}_0=-\frac{M}{\mathrm{i}\alpha\overline{U}_0+\beta\overline{C}_0\overline{U}_0/\overline{D}_0}, \quad \widehat{u}_0=\frac{-M(s_2\beta-\beta\overline{C}_0\overline{U}_0/\overline{D}_0)\widehat{v}_0+\lambda^2\overline{U}_0}{\mathrm{i}\alpha\left\{-s_2\beta\overline{C}_0+\beta\overline{C}_0\overline{U}_0/\overline{D}_0+\mathrm{i}\alpha\overline{U}_0^2-s_1\overline{C}_0\beta\overline{U}_0/\overline{D}_0\right\}}, \tag{3.15a}$$

$$\widehat{d}_0=-\frac{\overline{D}_0}{\mathrm{i}\lambda\overline{U}_0}\{\mathrm{i}\lambda\widehat{U}_0-M\widehat{v}_0\}. \tag{3.15b}$$

This equation is of course equivalent to (3.5) if $\overline{U}_0=\overline{D}_0=1$ and it is therefore possible to rescale (3.14) with all quantities now defined in terms of their local values. Since we are investigating the spatial instability problem, (3.14) must be solved at each value of

X in the range of interest for the complex wavenumber $\alpha(X)$. Since the zeroth-order problem contains no slow X derivatives on the disturbance field, the solution of this problem is unique only up to an arbitrary multiplicative factor $\widehat{h}_0(X)$ which must therefore be determined at higher order.

At order ϵ, we find that U_1, V_1, H_1 and D_1 satisfy

$$\mathrm{i}\alpha\overline{U}_0U_1+\mathrm{i}\alpha H_1+\frac{\beta}{D_0}\overline{C}_0(s_1U_1+s_2D_1)-\frac{\beta\overline{C}_0\overline{U}_0^2}{\overline{D}_0^2}D_1=\left(J_5\widehat{h}_0+J_6\frac{\mathrm{d}\widehat{h}_0}{\mathrm{d}X}\right)\mathscr{S}+\text{T.O.S.}, \quad (3.16a)$$

$$\mathrm{i}\alpha\overline{U}_0V_1+\frac{\partial H_1}{\partial y}+\frac{\beta}{\overline{D}_0}V_1\overline{C}_0\overline{U}_0=\left(J_7\widehat{h}_0+J_8\frac{\mathrm{d}\widehat{h}_0}{\mathrm{d}X}\right)\mathscr{C}+\text{T.O.C.}, \quad (3.16b)$$

$$\mathrm{i}\alpha(\overline{U}_0D_1+\overline{D}_0U_1)+\overline{D}_0V_{1y}=\left(J_3\frac{\mathrm{d}\widehat{h}_0}{\mathrm{d}X}+J_4\widehat{h}_0\right)\mathscr{S}+\text{T.O.S.}, \quad (3.16c)$$

$$-\frac{\mathrm{i}\Omega}{Q_0}\left(F_0^2H_1-D_1\right)+\mathrm{i}\alpha\overline{\Phi}_0(f_1U_1+f_2D_1)+\overline{\Phi}_0\left(\frac{V_{1y}}{\overline{U}_0}-R\frac{\partial^2}{\partial y^2}\left[F_0^2H_1-D_1\right]\right)$$
$$=\left(J_1\widehat{h}_0+J_2\frac{\mathrm{d}\widehat{h}_0}{\mathrm{d}X}\right)\mathscr{S}+\text{T.O.C.} \quad (3.16d)$$

Here, T.O.S. and T.O.C. denote terms which are orthogonal to $\mathscr{S}$ and $\mathscr{C}$, respectively, in $G\leqslant y\leqslant F$. These terms do not contribute to the solvability equation required to determine $\widehat{h}_0$ so we will not give these terms explicitly. The quantities J_1-J_8 are given in the Appendix. The solvability condition is most easily derived by defining

$$\boldsymbol{\eta}=\begin{pmatrix}V_1\\H_1\\S_1\\\partial S_1/\partial y\end{pmatrix}, \quad D_1=F_0^2H_1-S_1$$

so that (3.16) may be expressed as

$$\frac{\mathrm{d}\boldsymbol{\eta}}{\mathrm{d}y}=\begin{pmatrix}0&e_5&e_4&0\\e_8&0&0&0\\0&0&0&1\\0&e_7&e_6&0\end{pmatrix}\boldsymbol{\eta}+\begin{pmatrix}R_1\\R_2\\0\\R_3\end{pmatrix}, \quad (3.17)$$

Here, e_4-e_8 and R_1, R_2, R_3 are defined in the Appendix.

This equation must be solved subject to

$$\left.\begin{aligned}&\eta_1=F'\widehat{u}_0\widehat{h}_0, \quad y=F, \quad \eta_1=G'\widehat{u}_0\widehat{h}_0, \quad y=G,\\&\eta_4=0, \quad y=F,G.\end{aligned}\right\} \quad (3.18)$$

The adjoint of the homogeneous form of (3.17)–(3.18) has eigenvector

$$\widehat{x}_1(X)[\mathscr{S},\widehat{x}_2(X)\mathscr{C},\widehat{x}_3(X)\mathscr{C},\widehat{x}_4(X)\mathscr{S}]^T, \quad (3.19)$$

where

$$\widehat{x}_2=-M/e_8, \quad \widehat{x}_4=(M\widehat{x}_2-e_5)/e_7, \quad \widehat{x}_3=-M\widehat{x}_4.$$

Following the usual procedure, we obtain the solvability condition in the form

$$(F'-G')\widehat{u}_0\widehat{h}_0=\tfrac{1}{2}(F-G)(R_1+\widehat{x}_2R_2+\widehat{x}_4R_3),$$

which can be reduced to

$$\frac{\mathrm{d}\widehat{h}_0}{\mathrm{d}X} - \mu(X)\widehat{h}_0 = 0,$$

where $\mu(x)$ is defined in the Appendix. Note here that the terms denoted by T.O.C. and T.O.S. in (3.16) make no contribution to the solvability problem.

3.2. *The growth rate*

We define the growth rate $\sigma(X)$ in terms of the perturbation by writing

$$\sigma = \frac{\epsilon(\mathrm{d}/\mathrm{d}X)\{N(X)\}}{N},$$

where N is some averaged flow property. If, for example, we define the growth rate in terms of the average over y and t of the square of the (real) perturbation to the free surface height we have

$$N = \frac{\displaystyle\int_{2\pi/\Omega}\int_{G}^{F} \widetilde{H}^2 \,\mathrm{d}y\,\mathrm{d}t}{F-G},$$

then, after some manipulation, we find that σ_H, the growth rate based on the height of the free surface, is given by

$$\tfrac{1}{2}\sigma_H = -\alpha_i + \epsilon\mu_r(X) + O(\epsilon^2). \tag{3.20}$$

Similarly, the growth rate evaluated at the banks in terms of the water depth is given by

$$\sigma_D = -\alpha_i + \epsilon\mu_r(X) + \epsilon\left(\frac{\mathrm{d}\varkappa/\mathrm{d}X}{2\varkappa}\right) + O(\epsilon^2), \quad \varkappa = |\,\widehat{d}_0\,|^2, \tag{3.21}$$

and corresponding growth rates can be written down for the other flow quantities. We observe above that the growth rates associated with different flow quantities differ at $O(\epsilon)$ so that the neutral curves plotted correct to order ϵ will also depend on the flow quantity used to define it. Since the sediment depth, $F_0^2\widetilde{H} - \widetilde{D}$, is the most obvious record of a bar structure, we will use it to define the neutral configuration. Note also that if the background disturbance level in the channel is larger than ϵ then only the leading-order term in (3.21) is meaningful and the neutral curve is determined by the leading-order theory without a non-parallel effect.

We define a neutral point to be the position where the imaginary part of the growth rate is zero. In order to calculate the neutral points $\alpha(X)$, μ and $\widehat{d}_0$, etc. must be calculated numerically for a given basic state. If the imaginary part of α vanishes at $X = X_{n0}$, then we see from (3.20) that, correct to $O(\epsilon)$, the neutral point based on say the height of the free surface is given by

$$X = X_n = X_{n0} + \epsilon X_{n1} + \cdots, \quad X_{n1} = \frac{\left(\mu_r(X_{n0})_{X=X_{n0}}\right)}{\alpha_i'(X_{n0})}, \tag{3.22}$$

and the local value of β and Ω can then be defined in terms of basic flow quantities defined at X_n. Note, however, that we must retain higher-order terms in the expansion of α_i at a point where $\alpha_i' = 0$. Similar neutral points can be defined for the other flow properties. Before presenting our results, we note that the above discussion applies to a single mode for $m = 1, 3, 5, \ldots$. (These modes have the spanwise velocity component even about the mid-point of the channel.) In fact, the analysis given applies equally

well to odd modes with

$$U_0 H_0 D_0 \sim \cos\left(\frac{m\pi\hat{y}}{(F-G)/2}\right).$$

It can be shown that the analysis given above for the odd-mode growth rates applies to the even case if we change m to $-m$ with $m = 2, 4, 6, 8\ldots$. Finally, before we present our results, we make some remarks about the solution of the $O(\epsilon)$ system above. So far, we have only discussed the amplitude equation which results from the application of the solvability condition at this order. This amplitude equation determines the amplitude of the zeroth-order eigenfunction. In fact, we only showed explicitly the $O(\epsilon)$ forcing terms which contribute to the solvability condition. In addition, there are forcing terms at this order which force all the other odd and even modes. However, the corresponding differential systems do not require a solvability condition since they are all slaved to the wavenumber of the zeroth-order mode. Nevertheless this means that when the zeroth-order mode passes through a region of exponential growth, all other even and odd modes will grow exponentially at the same rate with relative amplitude $O(\epsilon)$ smaller. This means that when the wave enters a regime where one or more of the other modes are unstable, it will not have to amplify from the background level associated with naturally occurring disturbances.

4. Results and further discussion

In the first instance, we present results using only the leading-order approximation to the stability problem. This situation is most relevant to values ϵ smaller than typical magnitudes of background disturbance. At leading order, the growth rate is a function only of the width of the channel $F(X) - G(X)$ and it makes no difference whether or not the channel is symmetric. First, let us consider the channel

$$y = \pm 1, \quad X < 0, \quad y = \pm(1 + X), \quad 0 < X < 2,$$

used by FP in the Genoa experiments. Note that FP used a channel with walls diverging at a maximum inclination of 15° to the initial direction of the walls so an analysis is valid if $\tan 15°$ is sufficiently small for a small ϵ theory to be valid. However, it should be observed that the leading-order theory does not depend explicitly on ϵ so we do not have to give a numerical value for it at this stage. The neutral curves are then calculated by finding the downstream position where the growth rate of a particular mode vanishes and then the local value of the aspect ratio, frequency and wavenumber can be calculated in terms of the local flow properties. The local frequency and aspect ratio are given by

$$\beta_l = \beta\beta_\Delta, \quad \Omega_l = \Omega\Omega_\Delta,$$

where Ω_Δ and β_Δ are as defined in § 3. Figure 11 shows the first three 'local' neutral curves in the aspect ratio–frequency and distance–frequency planes for a typical case. In particular, we consider the situation when

$$F_0 = \sqrt{\tfrac{1}{2}}, \quad Q_0 = 0.3, \quad d_s = 0.01, \quad \Theta_0 C_0 = 0.3, \quad \beta = 5.$$

The curves labelled '1–2 swap' and '2–3 swap' denote the positions where the first mode and second mode become less unstable than the second and third modes, respectively. In figure 11(*b*), we have also indicated the downstream paths taken by constant-frequency disturbances as they propagate in the flow direction. We see that

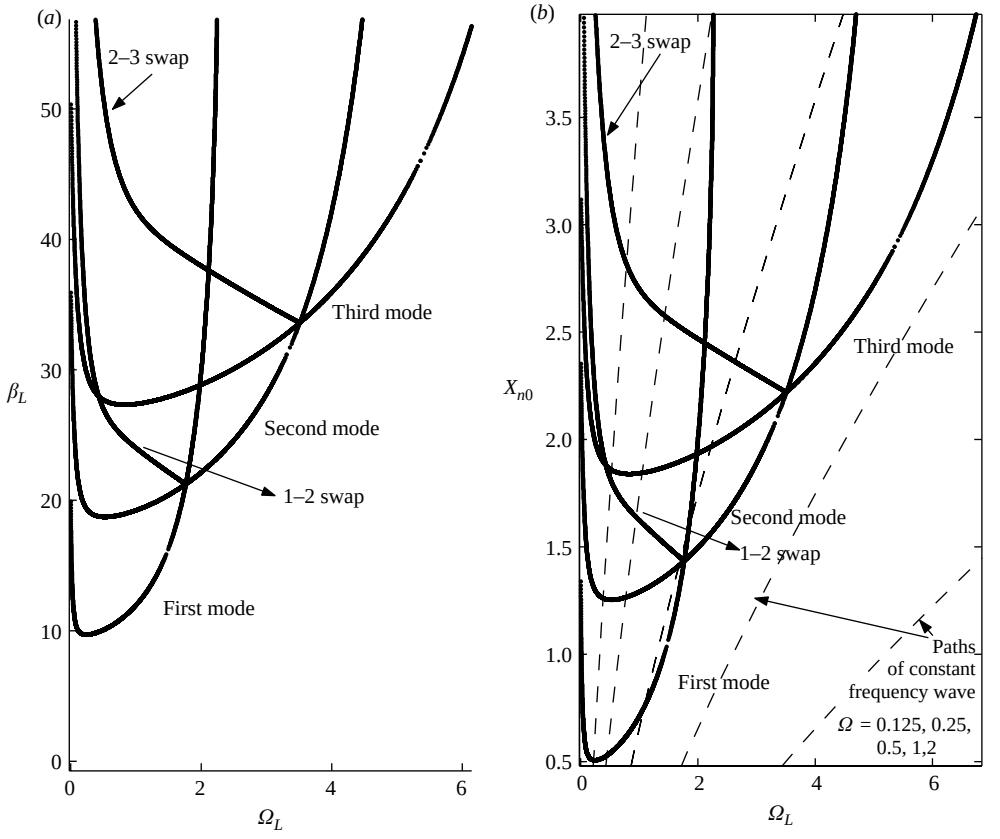

FIGURE 11. Neutral curves for $\Phi_0 = C_0\Theta_0 = 0.3$, $\beta = 0.5$, $r = 0.5$.

any path which passes into a region where the first mode grows quickly moves into a regime where the second mode is more unstable. This is, we believe, the reason why FP found that central bars were the preferred mode of instability in the set of experiments 1–8. Here, we are making an assumption implicitly made in the description of convectively unstable flows. Thus, we assume that upstream of the unstable region there is a dominant frequency in the flow which selects a particular combination of modes with that frequency. The part of the disturbance associated with the first mode will grow when it crosses the lowest curve in figure 11(*b*). However, if the disturbance does not grow sufficiently quickly for nonlinear effects to take over then the mode is then overtaken in size by the second mode as the disturbance passes into the region above the curve labelled '1–2 swap'. (Note that since the second mode is driven at $O(\epsilon)$ by the first mode, it will be swamped by the first mode within a distance of $O(\epsilon)$ of the 1–2 swap line). In the FP experiment, X varies in (0, 2), so the disturbances never reach a position where the third mode takes over. Of course, in cases where the first mode grows appreciably, then a finite-amplitude alternate bar could be set up before the central bar mode amplifies sufficiently to dominate the flow. This is only possible for very small dominant upstream frequencies which correspond to disturbance paths in figure 11(*b*) which at small values of the local frequency are almost vertical. Figure 11 suggests that in an experiment where X varies in (0, 3), the third mode will come into play.

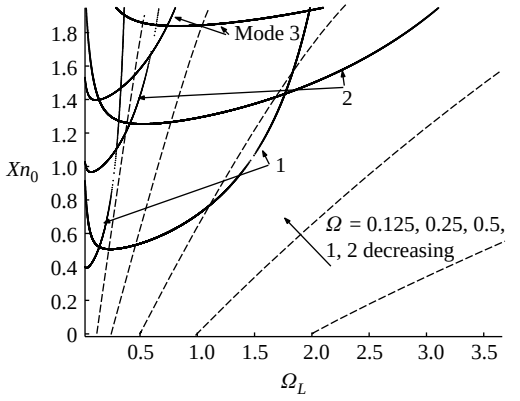

FIGURE 12. Neutral curves for $\Phi_0 = 0.3$, $\beta = 9$, $C_0\Theta_0 = 0.1, 0.3$ (smaller $C_0\Theta_0$ on left).

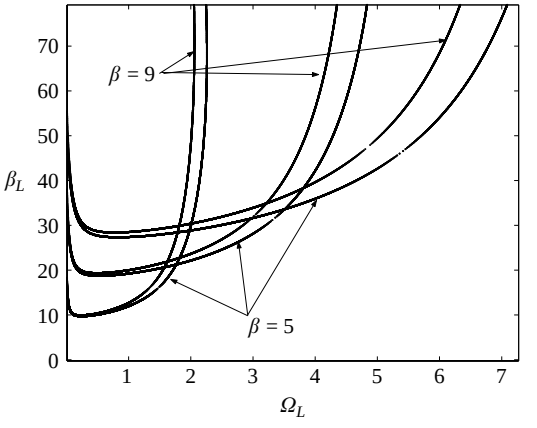

FIGURE 13. Effect of initial β on neutral curves for $\Phi_0 = C_0\Theta_0 = 0.3$.

Figure 12 shows the effect of the upstream Shield stress on the neutral positions for the first three modes. We see here that a significant effect of decreasing the upstream Shield stress is to reduce greatly the band of frequencies which are amplified. If the frequencies present in the incoming flow are comparable in the two situations, this suggests that the first mode will become more inaccessible as the upstream Shield stress falls.

Figure 13 presents the same results as shown in figure 11 at a higher value of the upstream aspect ratio. We see that the upstream aspect ratio has little effect on the neutral configuration plotted in terms of β_l and Ω_l. Note, however, that if the upstream value of the aspect ratio is decreased sufficiently, then only part of the unstable region will be reached as a wave moves downstream. However, the results of figure 10 suggest that at even higher values of X, the third mode (and indeed even higher modes) will come into play.

Figure 14 shows the effect of Froude number on the instability. Thus, we present results for the case $F_0 = \sqrt{1/2}, 1.3$, $Q_0 = 0.3$, $\Theta_0 C_0 = 0.3$, $\beta = 5$. Figure 14(a) shows that when the results are plotted in the (β_l, Ω_l)-plane, the upstream Froude number has very little effect on the results. However, figure 14(b) shows that the effect is more noticeable if we plot results in the (X, Ω_l)-plane. Here we see that instability begins

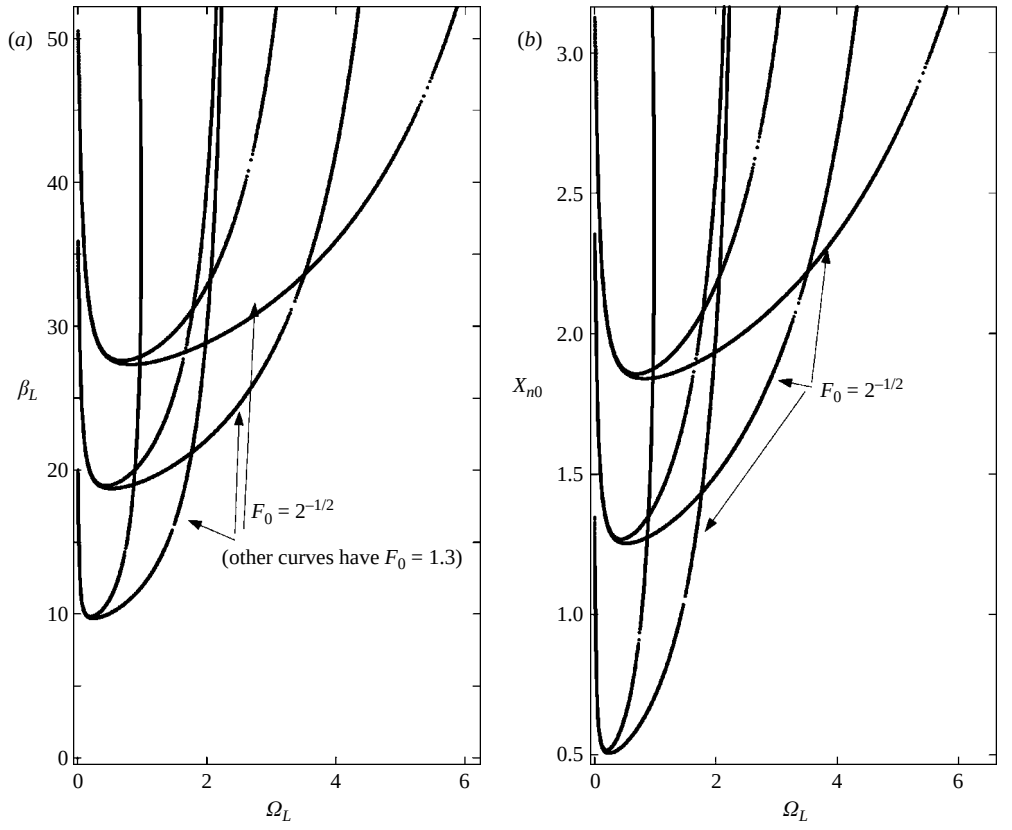

FIGURE 14. The effect of the upstream F_0 on the neutral curves for $\Phi_0 = C_0\Theta_0 = 0.3$, $\beta = 5$.

earlier at higher Froude numbers and that the higher modes are therefore more likely to be experimentally accessible in that regime.

Now we present the results from the leading-order stability theory for the channel defined by (2.29). In these calculations, we have taken $A = 0.5, 1, 1.5, 2$ and the other constants are given by

$$F_0 = 0.75, \quad Q_0 = 0.3, \quad \Theta_0 C_0 = 0.3, \quad \beta = 5.$$

Figure 15 shows the first mode neutral curves for these cases. Not surprisingly, figure 15(*a*) shows that the flow first becomes unstable to the largest-amplitude expansion. Note here that each calculation gives two curves corresponding to the onset of instability as the channel expands and its stabilization as the channel contracts further downstream. However, figure 15(*b*) shows the remarkable result that, if the results are plotted in the (β_L, Ω_L)-plane, the results corresponding to the onset and cessation of instability at all amplitudes become graphically indistinguishable if we work with the aspect ratio as the control parameter. Indeed, we have in figure 15(*b*) also plotted the neutral curves for the linearly diverging channel at the same values of the flow parameters and we see that in the aspect ratio–frequency plane the results are indistinguishable from the present case. Now let us see how the above conclusions are modified if we allow for the $O(\epsilon)$ correction to the growth rates. The parameter values used above are typical of those to be found in the field, now we turn our attention in detail to the experimental results of FP.

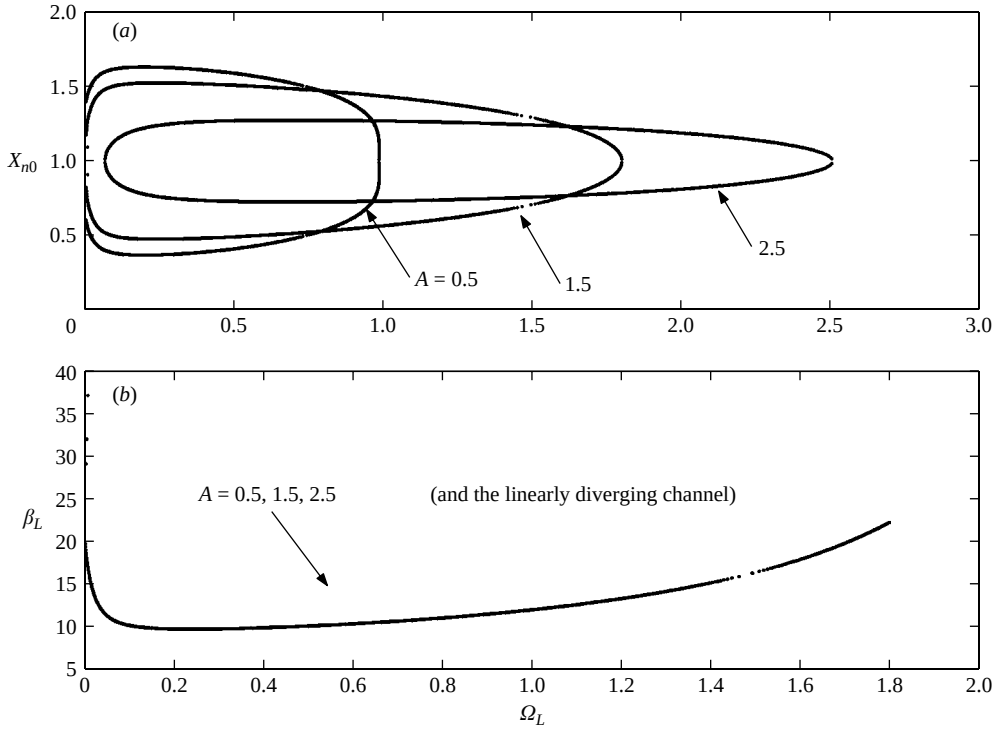

FIGURE 15. The neutral curves for the locally dilated channel.

We recall that the first eight experiments reported by FP corresponded to the linearly divergent channel defined by

$$y = \pm 1, \quad X < 0, \quad y = \pm(1 + X), \quad 0.0 < X < 2.$$

The eight runs with which we can compare our theory typically correspond to values of Q_0 lower than those to be found in the field. In fact, this parameter can be absorbed directly into the frequency so we can in effect scale out its effect on the stability problem. For that reason, we will now plot neutral curves using Ω_L/Q_0 rather than Ω_L. Figures 16 and 17 show the neutral curves for the first three modes for the experimental configuration of FP. Figure 16 shows the results in the frequency–X_n plane whilst figure 17 uses the local aspect ratio as a control parameter. Figure 16 shows results qualitatively similar to those found above, although the results for experiments 4 and 6 deserve some comment. The upstream aspect ratios for these cases were 10 and 7, respectively. FP state that all upstream values of the aspect ratio were in the stable regime, but figure 16(d) clearly shows instability occurring at the entrance to the divergent reach. The effect is also present in figure 16(f) where we see instability occurring very soon after the wave enters the channel.

Figure 17 again demonstrates the early onset of instability in two of the experiments. A fixed-frequency wave moves along well-defined paths in these figures. Figure 17(i) shows such paths for experiment (1) of FP. We observe that a wave which is unstable to the first mode rapidly becomes stable to that mode and unstable to the second as it moves downstream. This is crucial because we believe this is the reason why divergent channels are able to sustain central bar modes initially associated with forcing caused

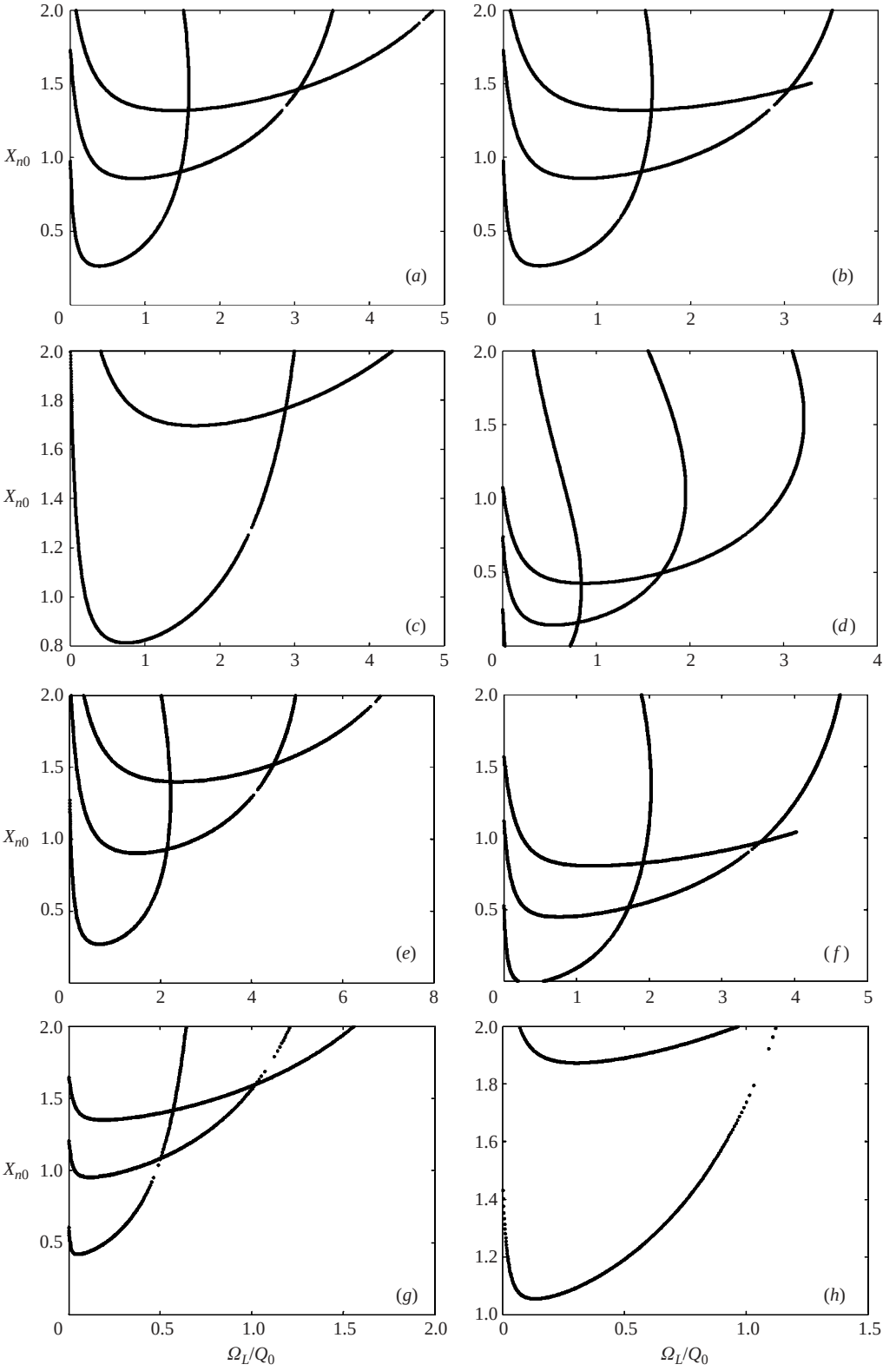

FIGURE 16. The neutral curves against local frequency for the FP experiment. (*a*)–(*h*) Experiments 1–8.

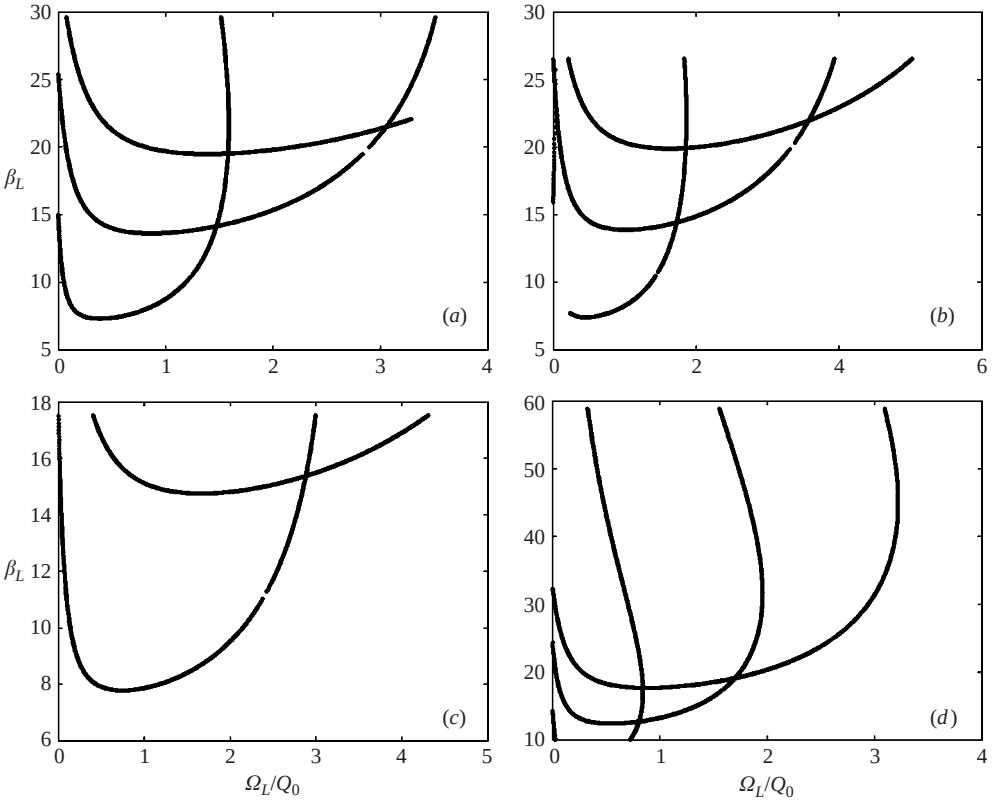

FIGURE 17(*a–d*). For caption see facing page.

by the channel divergence (i.e. the second mode) rather than alternating bars. In order to see why this is the case, we now discuss the results presented in figures 18 and 19. Figure 18 shows the growth rates for five different frequency modes (first and second) as they move downstream in the configuration of experiment (1). We see that the first modes amplify first, but then become overtaken by second modes before eventually becoming stable. Note that the second mode growth rates are higher than those of the first. The upshot of the last observation is that if, as shown in figure 19, we compute the integrated growth of a mode from the point where it becomes unstable by writing

$$J = -\int_{X_n}^{X} \alpha_i(s)\,\mathrm{d}s,$$

then the second modes undergo significantly more amplification than the corresponding first modes as they move downstream. Moreover, since the incoming flow has a steady central bar, a receptivity calculation of the type given by Hall (2004) will predict that the central bar will be preferentially excited. (We will return to this point later when we draw some conclusions.) Indeed, since the amplification of a disturbance is in fact $\mathrm{e}^{J/\epsilon}$, then in a divergent channel with small background disturbances requiring significant amplification before a finite-amplitude state is achieved, it is much more likely that it will be second modes which achieve the required amplitude. We believe that this is the reason for the experimentally observed preference for central bars found by FP.

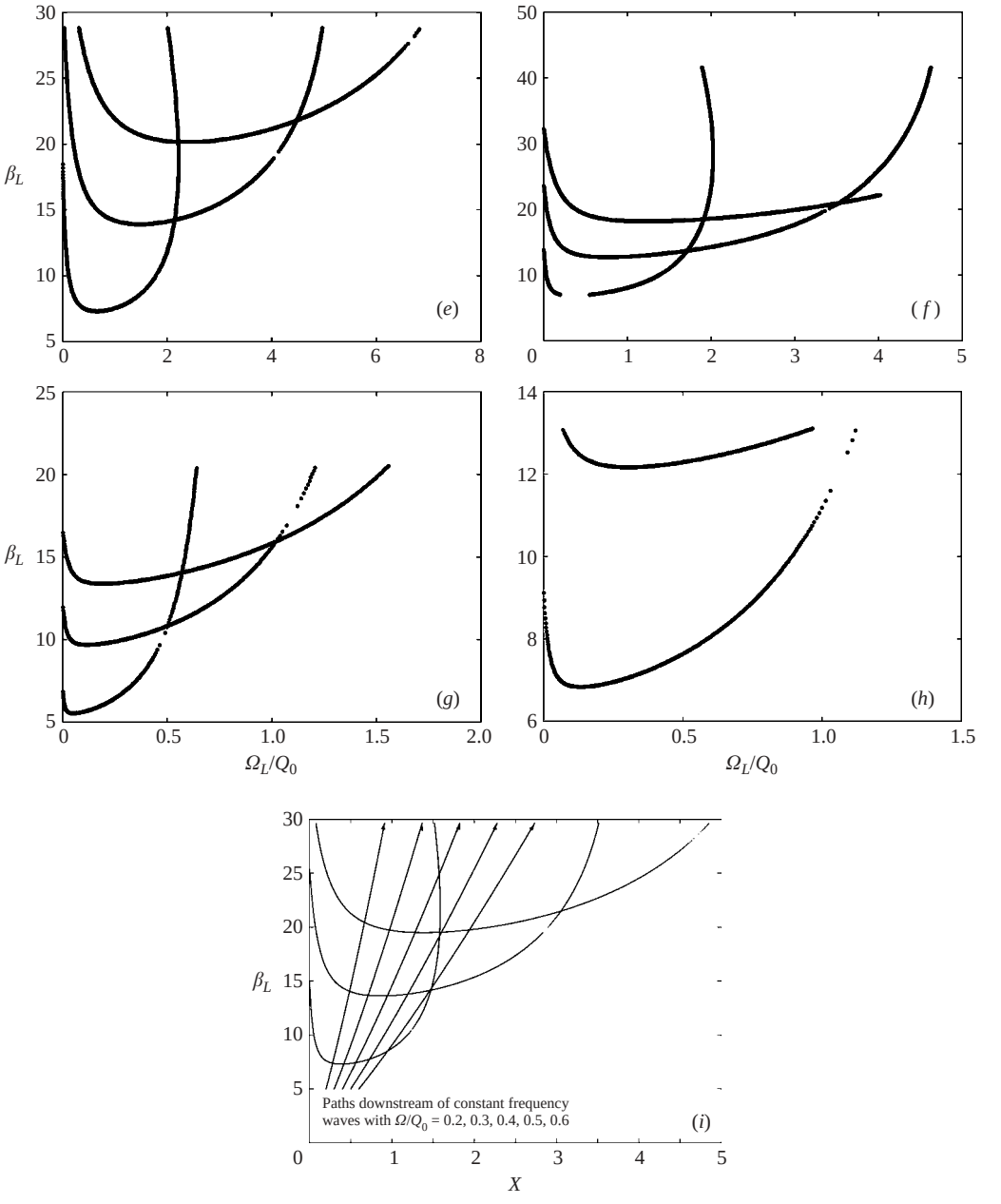

FIGURE 17. The neutral β against frequency for the FP experiment. (*a–h*) Experiments 1–8. (i) Paths of constant frequency waves for the configuration of experiment (1) of FP.

The results presented so far have been restricted to predictions based on the leading-order approximation to the neutral point. Now we present results which indicate the effect of the order ϵ correction term associated with the growth rate defined on sediment depth. We recall that figure 17 corresponded to the leading-order predictions of the neutral locations for the eight experimental investigations of FP. Figure 20 shows the first mode neutral curves for experiment 1 from FP when the next

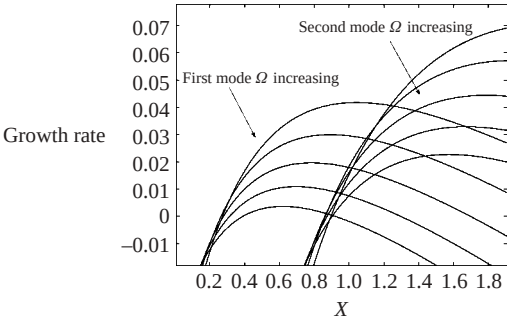

FIGURE 18. Growth rates of first two modes for $\Omega/O_0 = 0.2, 0.3, 0.4, 0.5, 0.6$.

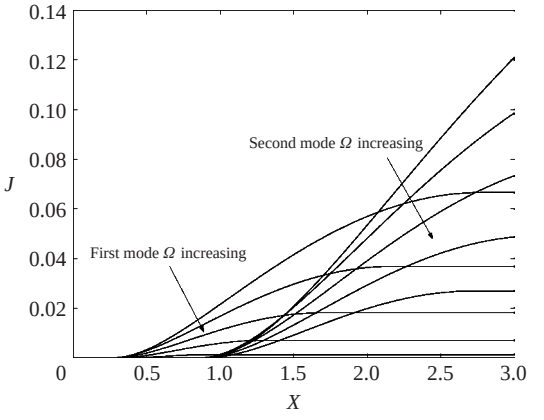

FIGURE 19. Integrated growth for first two modes $\Omega/O_0 = 0.2, 0.3, 0.4, 0.5, 0.6$.

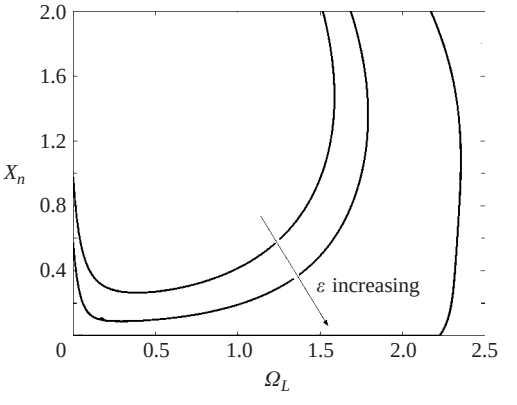

FIGURE 20. The first mode non-parallel neutral curves for FP experiment 1, $\varepsilon = 0, 0.01, 0.04$.

order correction term is taken into account. The neutral curves shown correspond to $\varepsilon = 0.0, 0.01, 0.04$. We observe that, in all cases, flow divergence has a destabilizing effect on the flow stability with the unstable regime of the different modes increased in size. In fact, even at these quite small values of the slope, there is a large effect and the theory is probably not valid even at the smallest value of the slope used in the FP experiments. We see that when $\epsilon = 0.04$ the flow is destabilized at the very beginning

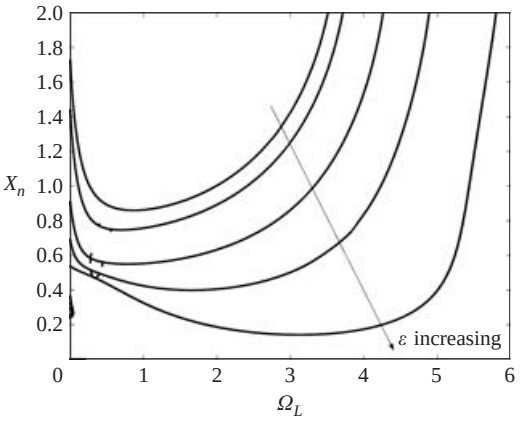

FIGURE 21. The second mode non-parallel neutral curves for FP experiment 1, $\varepsilon = 0, 0.01, 0.04, 0.08, 0.15$.

of the divergent reach of the flow. Thus, at sufficiently high values of the slope, the neutral curve become discontinuous. However, it is likely that the range of validity of the theory does not extend to the higher values of the slope used since the changes in the positions of the neutral curves are $O(1)$. Figure 21 gives the corresponding second mode results for the first experiment of FP. We again note the destabilizing effect of flow divergence though the effects are somewhat less than was the case for the first mode. We note once again that, at sufficiently high slopes, the flow is immediately unstable. It is also noticeable that the range of unstable wavenumbers for the second mode is increased significantly more than is the case for the first mode. Calculations for the other experimental configurations of FP produce essentially the same effects seen in figures 20 and 21.

In summary, we conclude that the asymptotic theory we have developed agrees very well with FP, but the slowly varying description of the instability problem is probably not valid at the wall slopes used by FP. Our results show that a 1% wall slope produces a change in the neutral curve of size 10%, so even at the smallest experimentally used slope, 0.26, we are predicting changes in neutral values of the width comparable with its parallel value. Nevertheless the small slope theory indicates the effect likely to be observed at the experimentally used values. Thus, we expect the first two modes to be significantly destabilized and the unstable band of frequencies to be increased significantly for the second mode. The path of a constant-frequency wave as it moves downstream is the same whether or not we use the $O(\varepsilon)$ correction term to define the growth rate. Thus, our conclusion that the flow divergence effectively means that waves move rapidly into the region dominated by the second mode becomes unchanged. Indeed, the widening of the unstable second-mode frequency band accentuates that effect.

5. Conclusions

(i) In a slowly diverging channel, a steady central bar with slope in the spanwise direction of size ϵ^2 is forced. This slope at any spanwise location increases monotonically from zero at the beginning of the divergent region.

(ii) In a diverging channel, linear instability suggests that second-mode disturbances are likely to be more amplified than alternating bars as they move downstream. At high enough values of the local width ratio each of the modes can be stationary and again the steady central mode is likely to be most amplified.

(iii) The central bars found by FP are likely to be associated with the forced steady central bars. At first sight, it might therefore seem that the instability theory is not relevant to the FP experiment. However, these central bars will selectively initiate steady central bars when the flow becomes unstable through the receptivity process discussed by Hall (2004). In that paper, it was shown that flow oscillations of size A_1 upstream of width variations of size A_2 produce migrating instability waves of size A_1A_2. Stationary modes which are possible at relatively high values of the width ratio are of size A_2. Thus, in situations where steady central bar modes are unstable they are preferentially excited in the receptivity process. This is, we believe, the situation in the FP experiments with the central bars initially forced by flow divergence moving into a region where they are unstable, at which stage their relative size and growth rates ensure that they survive throughout the divergent region. This is exactly the situation in a three-dimensional boundary where stationary crossflow vortices tend to be generated in preference to travelling vortices because the stationary modes are generated more efficiently by surface imperfections.

This work was partially carried out whilst the author was a visitor at CESPR and CSIT, Florida State University. The author wishes to thank the referees for many useful suggestions on the first draft of this paper and Professor David Furbish for helpful comments.

Appendix

In order to define the functions $J_1 - J_8$ appearing in (3.16) we first define $\Delta_1 - \Delta_8$, N, by

$$\overline{V}_0\mathscr{C} = \Delta_1\mathscr{S} + \text{T.O.S.}, \quad \overline{V}_{0y}\mathscr{S} = \Delta_2\mathscr{S},$$
$$\overline{V}_0\mathscr{S} = \Delta_3\mathscr{C} + \text{T.O.C.}, \quad \overline{V}_{0y}\mathscr{C} = \Delta_4\mathscr{C},$$
$$y\mathscr{C} = \Delta_5\mathscr{S} + \text{T.O.S.}, \quad y\mathscr{S} = \Delta_6\mathscr{C} + \text{T.O.C.},$$
$$\overline{D}_1\mathscr{C} = \Delta_7\mathscr{C} + \text{T.O.S.}, \quad \overline{D}_1\mathscr{S} = \Delta_8\mathscr{S} + \text{T.O.C.},$$

$$N = m\pi/(F-G)'/(F-G)^2,$$

where T.O.C. and T.O.S. were defined earlier and $\Delta_5 = \Delta_6 = (-1)^{m+1}(F-G)/(2m\pi)$, $\Delta_2 = \Delta_4 = -(\overline{U}_0\overline{D}_0)_X/\overline{D}_0$, $\Delta_1 = \Delta_3 = \Delta_4\Delta_5$. The quantities $J_1 - J_{12}$ and $R_1 - R_3$ may then be written in the form

$$J_1 = -\frac{\mathrm{i}\alpha\overline{\Phi}_0\Delta_1 f_1\widehat{v}_0}{\overline{U}_0} - \frac{\mathrm{i}\alpha\overline{\Phi}_0\Delta_1}{\overline{U}_0}\left[\frac{\widehat{v}_0}{\overline{U}_0} - MR\left(F_0^2 - \widehat{d}_0\right)\right]$$
$$+ \overline{\Phi}_{0X}[f_1\widehat{u}_0 + f_2\widehat{d}_0] + \Phi_0[f_{1X}\widehat{u}_0 + f_{2X}\widehat{d}_0] - \frac{\overline{\Phi}}{\overline{U}_0^2}(\widehat{u}_0\Delta_2 + M\widehat{u}_0\Delta_1)$$
$$- \frac{\Delta_3\overline{\Phi}_0}{\overline{U}_0}(Mf_1\widehat{u}_0 + Mf_2\widehat{d}_0) + \Phi_0(f_1\widehat{u}_{0X} + f_2\widehat{d}_{0X}),$$
$$- N\Phi_0\Delta_5(f_1\widehat{u}_0 + f_2\widehat{d}_0) - \left[\mathrm{i}d\widehat{v}_0 A + \beta\widehat{v}_0 U_0\left[\frac{C_0(D_0)}{D_0}\right]' + \beta\widehat{v}_0 A\frac{C_0}{D_0}\right]\Delta,$$

$$J_2 = -\overline{\Phi}_0(f_1\widehat{u}_0 + f_2\widehat{d}_0),$$
$$J_3 = -\overline{U}_0\widehat{d}_0 - \overline{D}_0\widehat{u}_0,$$
$$J_5 = -\overline{U}_0\widehat{u}_{0X} - \widehat{u}_0\frac{\mathrm{d}\overline{U}_0}{\mathrm{d}X} - \Delta_1\widehat{u}_0 M + \overline{U}_0 N\Delta_5\widehat{u}_0 - \frac{\beta\overline{C}_0\widehat{v}_0\Delta_1}{\overline{D}_0} + N\Delta_5$$
$$- [\mathrm{i}\partial(A\widehat{d}_0' + \widehat{u}_0) - M\widehat{v}_0]\Delta_8$$
$$J_4 = -\overline{U}_0\widehat{d}_{0X} - \overline{D}_0\widehat{u}_{0X} - \widehat{u}_0\frac{\mathrm{d}\overline{D}_0}{\mathrm{d}X} - \widehat{d}_0\frac{\mathrm{d}\overline{U}_0}{\mathrm{d}X} - \Delta_1 M\widehat{d}_0 - \Delta_2\widehat{d}_0 + N\widehat{d}_0\overline{U}_0\Delta_5 + N\overline{D}_0\Delta_5\widehat{u}_0$$
$$- \left[\mathrm{i}dA\widehat{u}_0 + \beta(s_1\widehat{u}_0 + s_2\widehat{d}_0)\left\{\left(\frac{\overline{C}_0(D_0)}{D_0}\right)' + 2U_0A\frac{\overline{C}_0^1}{\overline{C}_0} + U_0^2\left(\frac{\overline{C}_0(D_0)}{D_0}\right)'\right\}\right.$$
$$\left. + 2\frac{\beta\overline{C}_0}{D_0}A\widehat{U}_0 - \beta\left\{\left(\frac{\overline{C}_0(D_0)}{D_0}\right)' U_0^2 + \frac{2\overline{C}_0U_0}{D_0^2}A\right\}\widehat{d}_0\Delta_7\right]$$
$$J_6 = -1 - \overline{U}_0\widehat{u}_0,$$
$$J_7 = -\overline{U}_0\widehat{v}_{0X} + M\widehat{v}_0\Delta_3 - \widehat{v}_0\Delta_4 - \frac{\beta}{\overline{D}_0}(\overline{C}_0'\overline{U}_0\Delta_3\widehat{d}_0 + \overline{C}_0\widehat{u}_0\Delta_3) - \overline{U}_0N\Delta_6\widehat{v}_0 + \frac{\beta\widehat{d}_0}{\overline{D}_0^2}\overline{C}_0\overline{U}_0\Delta_3,$$
$$- \left[4\mathrm{i}d\overline{\Phi}_0''\Theta_0^2\overline{C}_0^2U_0^2\left[\widehat{u}_0 + \frac{U_0\overline{C}_0'\widehat{d}_0}{2\overline{C}_0}\right]\left[A + \frac{U_0\overline{C}_0'}{2\overline{C}_0}\right]\right.$$
$$+ 2\mathrm{i}d\overline{\Phi}_0'\Theta_0\left[\widehat{u}_0(\overline{C}_0A + U_0\overline{C}_0') + \widehat{d}_0\left(U_0A\overline{C}_0' + \tfrac{1}{2}U_0^2\overline{C}_0\right)\right]\Delta_7$$
$$\left. - \left[\Phi_0'\left(\frac{-M\widehat{v}_0}{U_0} + RM^2\left[F_0^2 - \widehat{d}_0\right]\right)\Theta_0\left(2\overline{C}_0U_0A + \overline{C}_0U_0^2\right) + \overline{\Phi}_0\frac{MA\widehat{v}_0}{U_0^2}\right]\Delta_7\right]$$
$$J_8 = -\overline{U}_0\widehat{v}_0, \quad J_9 = \frac{J_3}{\overline{D}_0} - J_6, \quad J_{10} = \frac{J_4}{\overline{D}_0} - J_{5,11},$$
$$J_{11} = \left(f_1 - \frac{1}{\overline{U}_0}\right)\frac{J_5}{R} + \frac{J_4}{R\overline{D}_0\overline{U}_0} - \frac{J_1}{R\Phi_0}, \quad J_{12} = \left(f_1 - \frac{1}{\overline{U}_0}\right)\frac{J_6}{R} + \frac{J_3}{R\overline{D}_0\overline{U}_0} - \frac{J_2}{R\Phi_0},$$
$$R_1 = J_9\widehat{h}_0' + J_{10}\widehat{h}_0, \quad R_2 = J_8\widehat{h}_0' + J_7\widehat{h}_0, \quad R_3 = J_{12}\widehat{h}_0' + J_{11}\widehat{h}_0.$$

The quantities e_0, e_1, e_2, etc. are defined by

$$e_0 = \mathrm{i}\alpha\overline{U}_0 + \frac{\beta\overline{C}_0s_1}{\overline{D}_0}, \quad e_2 = -\frac{\mathrm{i}\alpha}{e_0}, \quad e_2 = \frac{-\beta\overline{C}_0s_2/\overline{D}_0 + (\beta/\overline{D}_0^2)\overline{C}_0\overline{U}_0^2}{e_0},$$
$$e_3 = e_1 + e_2F_0^2, \quad e_4 = \frac{\mathrm{i}\alpha\overline{U}_0}{\overline{D}_0} + \mathrm{i}\alpha e_2, \quad e_5 = -\mathrm{i}\alpha e_3 - \frac{\mathrm{i}\alpha\overline{U}_0F_0^2}{\overline{D}_0},$$

$$e_6 = \left(-\frac{\mathrm{i}\Omega}{\overline{\Phi}_0Q_0} + \frac{e_4}{\overline{U}_0} - \mathrm{i}\alpha[f_1e_2 + f_2]\right)\Big/R, \quad e_7 = \left(\frac{e_5}{\overline{U}_0} + \mathrm{i}\alpha\left[f_1e_3 + f_2F_0^2\right]\right)R,$$

$$e_8 = -\left(\mathrm{i}\alpha\overline{U}_0 + \frac{\beta\overline{C}_0\overline{U}_0}{\overline{D}_0}\right).$$

Finally, the quantity μ is defined by

$$\mu = \frac{2(F' - G')\widehat{u}_0/(F - G) - J_9 - \widehat{x}_2J_7 - \widehat{x}_4J_{11}}{J_{10} + \widehat{x}_2J_8 + \widehat{x}_4J_{12}}.$$

REFERENCES

Ashmore, P. E. 1982 Laboratory modelling of gravel braided stream morphology. *Earth Surface Proc. Landforms* **7**, 289–317.

Ashmore, P. E. 1991 How do gravel-bed rivers braid? *Can. J. Earth Sci.* **28**, 326–341.

Blondeaux, P. & Seminara, G. 1985 A unified bar-bend theory of river meanders. *J. Fluid Mech.* **157**, 449–470.

Bolla Pittaluga, M., Repetto, R. & Tubino, M. 2003 Channel bifurcation in braided rivers: equilibrium configurations and stability. *Water Resour. Res.* **39**, 1046, doi:10.1029/2001WR001112.

Colombini, M., Seminara, G. & Tubino, M. 1987 Finite-amplitude alternate bars. *J. Fluid Mech.* **181**, 213–232.

Engelund, E. & Hansen, F. 1967 A monograph on sediment transport in alluvial streams. Danish Technical Press, Copenhagen.

Federici, B. & Paola, C. 2003 Dynamics of bifurcations in noncohesive sediments. *Water Resources* **39**, 1032 (referred to herein as FP).

Federici, B. & Seminara, G. 2003 On the convective nature of bar instability. *J. Fluid Mech.* **487**, 125–145.

Gaster, M. 1974 On the effects of boundary-layer growth on flow stability. *J. Fluid Mech.* **66**, 465–480.

Hall, P. 2004 Alternating bar instabilities in unsteady channel flows over erodible bed. *J. Fluid Mech.* **499**, 49–73.

Leopold, L. B. & Wolman, W. G. 1957 River channel patterns: braided, meandering and straight. *US Geological Survey Professional Paper*, 282-B, 39–85.

Kinoshita, R. 1961 Investigation of channel deformation in Ishikari river. *Rep. Bureau of Resources.* Dept of Science and Technology, Japan.

Repetto, R., Tubino, M. & Paola, C. 2003 Planimetric instability of channels with variable width. *J. Fluid Mech.* **457**, 79–109.

Tubino, M. & Seminara, G. 1990 Free-forced interactions in developing meanders and suppression of free bars. *J. Fluid Mech.* **214**, 131–159.